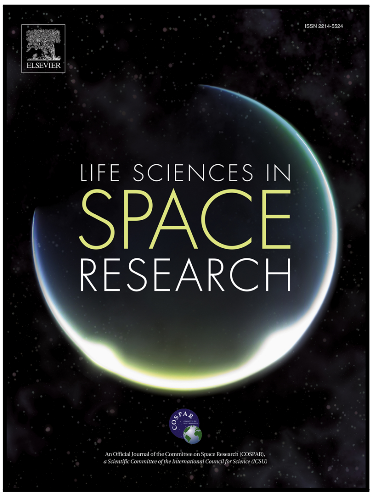

Neutron dosimetry on the International Space Station using a routine track etch personal dosemeter: neutron dose assessments within the HAMLET project

LG Hager , JS Eakins , RJ Tanner , T Berger , D Matthiä

PII: S2214-5524(26)00095-7
DOI: https://doi.org/10.1016/j.lssr.2026.06.004
Reference: LSSR 721

To appear in: *Life Sciences in Space Research*

Received date: 4 February 2026
Revised date: 2 June 2026
Accepted date: 16 June 2026

Please cite this article as: LG Hager , JS Eakins , RJ Tanner , T Berger , D Matthiä , Neutron dosimetry on the International Space Station using a routine track etch personal dosemeter: neutron dose assessments within the HAMLET project, *Life Sciences in Space Research* (2026), doi: https://doi.org/10.1016/j.lssr.2026.06.004

Neutron dosimetry on the International Space Station using a routine track etch personal dosemeter: neutron dose assessments within the HAMLET project

Hager L G[1,*], Eakins J S[1], Tanner R J[1], T Berger[2] and D Matthiä[2]

[1] UK Health Security Agency (UKHSA), Chilton, Didcot, OXON, OX11 0RQ, United Kingdom
[2] Deutsches Zentrum für Luft- und Raumfahrt e.V. (DLR), 51147 Köln, Germany

Abstract

Standard issue track etch neutron personal dosemeters have been used for measurements on board the International Space Station (ISS), but routine dose reporting is not possible because the radiation environment in the ISS is complex: additional methods are required beyond those used normally, to help identify and discard the signal that is due to charged particles that were not produced by neutron interactions. A different calibration is also required for the neutron-induced component of the signal because the neutron field extends to much higher energies than those encountered routinely in terrestrial workplaces. The analytical methods applied to make the necessary corrections are described in detail in this paper and some of the limitations are discussed. Use of these methods allows an estimate to be made of the neutron component of dose within the ISS environment. Specifically, measurements made during the ESA MATROSHKA contract and its subsequent scientific exploitation during the EC HAMLET project, are presented. Assessed neutron effective dose rates were in the range 58 μSv d^{-1} to 151 μSv d^{-1}. Original dose estimates from model calculations performed during HAMLET are compared to that obtained by using recent environmental and radiation transport models, but the effect on the dose estimate is shown to be negligible.

1 INTRODUCTION

Excepting the very rare instances of criticality accidents, astronauts receive the highest neutron doses of any profession. The neutron fields to which astronauts are exposed are higher in energy and more isotropic than the fields that other workers receive, and there are complicating factors arising from the many other types of particles that are components of those fields. In most conventional workplaces, etched-track neutron personal dosemeters have a signal that is caused solely by neutrons incident on the dosemeter, aside from any intrinsic background. For astronauts we cannot assign the net signal simply to the neutron exposure, and hence failure to remove unwanted component of the signal from the dose assessment causes overestimates of the astronaut's total dose. Further discussion on this is found in NCRP Report 142 (2002) and ICRP Publication 123 (2013), where detection methods for estimating and discriminating the different radiation species in Low Earth Orbit (LEO) are discussed.

For astronauts, there is always likely to be a significant neutron fluence present, and accurate estimation of the neutron dose is a primary concern. Despite the importance of these dose estimations, the small number of astronauts makes the development of specific neutron personal dosemeters for astronauts unviable. The approach discussed here is hence the use of a standard neutron personal dosemeter with adjusted response and subtractions of unwanted signals to improve the accuracy of the neutron dose estimation.

The radiation fields considered are not perturbed by solar particle events, which would boost the fluence of protons considerably for a period of a few hours. The reason for doing this is that they are very short duration compared to the total flight duration, and there were very few significant events between GLE #69 (December 2005) and GLE #77 (November 2025).

The United Kingdom Health Security Agency (UKHSA) and its forerunner organisations have been involved in the assessment of cosmic radiation doses for many years. Involvement with the EC-DOSMAX contract (2000 – 2004) https://cordis.europa.eu/project/id/FIGM-CT-2000-00068) saw the use of the UKHSA's track etch and thermoluminescent personal dosemeters to evaluate civil aircrew doses from cosmic radiation during solar maximum. Low Earth orbit neutron doses have been assessed on the International Space Station (ISS), initially via NASA shuttle missions (2000-2009), then during the ESA MATROSHKA contract (2003-2009), and under contract to the German Aerospace Centre (DLR) for astronaut doses (2006-present). Typically, astronaut doses from the charged particle and photon components are measured separately by other dosimetry systems incorporated into the overall measurement campaign.

This paper describes methods used by the UKHSA to assess neutron doses inside the International Space Station (ISS). The methodology was originally developed to support the experimental phases of the EC 7th Framework Programme (FP7) funded HAMLET project ("*Human Model MATROSHKA for Radiation Exposure Determination of Astronauts*") (Reitz *et al*, 2009), in which dosemeters were positioned upon the European Space Agency (ESA) MATROSHKA phantom (MTR) (Reitz and Berger, 2006) flown onboard the ISS (Berger *et al*, 2013); brief summary details of those experiments are given in Table 1. The culmination of UKHSA's contribution to this project was a work package report (Hager *et al*, 2011), which assessed the neutron doses to an anthropomorphic phantom. Subsequently, the method has been used for the assessment of doses to astronauts wearing the ESA European Crew Personal Dosemeter, EuCPD (Straube *et al*, 2010).

Table 1
Location of the MATROSHKA phantom on the ISS during the three experimental phases

MTR Phase	Location	Mean Solar heliocentric potential	Duration days
1	Outside Zvezda module	608 MV	539
2A	Inside Pirs docking compartment DC-1	400 MV	336
2B	Inside Zvezda service module	302 MV	404

The standard issue UKHSA Poly Allyl Diglycol Carbonate (PADC) neutron personal dosemeter (Gilvin *et al*, 2001) was used for these assessments. Neutrons are detected using the damage trail, called a 'latent track', caused by charged particle secondaries produced from interactions in the detector and holder. Electrochemical etching of these tracks can produce white "spots" near the surface, known as pits, as shown in Fig. 1. Electrochemical etching processes one face of the detector only: the back face (or 'rear surface').

The standard analysis technique for routine personal dosimetry with the neutron PADC dosemeter is to perform an electrochemical etch, scan the detector using a commercial digital photographic slide scanner, and then automatically count the pits using customised software (Bartlett *et al*., 1997; Steele *et al*., 1999; Tanner *et al*., 2001, Hager *et al*., 2017); a linearity correction and background subtraction is then applied. This method counts, without discrimination, all particles with $\mathrm{LET}_{\infty,\ \mathrm{PADC}}$ > ~40-60 keV μm^{-1} crossing the etched volume of the detector.

The UKHSA PADC dosemeter is optimized for assessing neutron doses in the terrestrial workplace, having a well characterised fluence-energy response covering the typical terrestrial workplace neutron energy range (Gilvin *et al*, 2001). Additional techniques and extensions to its characterization are therefore needed if it is to be used within the complex space radiation environment. Moreover, the UKHSA dosemeter is only intended to detect the signal that derives from the neutron component of the ISS field, but any charged particles incident on the dosemeter or anthropomorphic phantom or astronaut can potentially also contribute to the signal. This is problematic for measurements on the ISS, as unlike the terrestrial workplace, there is an abundance of primary charged particles present. The tracks on the dosemeter that are caused by these charged particles therefore need to be identified, and then subtracted, to correctly resolve the signal due to just the neutrons. The current paper describes the methods employed by UKHSA to account for the unwanted signal, and in turn derive the appropriate neutron dose response characteristic for the UKHSA PADC dosemeter for use on board the ISS, such that neutron doses may be assessed accurately. In addition to this description of the general method, its specific application to the MATROSHKA data evaluation within the HAMLET project will also be presented in this paper. In turn, results will be provided for the neutron components of dose that were obtained for the MATROSHKA phases on the ISS.

One important step towards recharacterizing the UKHSA dosemeter involves an evaluation of the multi-particle radiation field within the ISS. This was achieved by a process of Monte Carlo simulation, based on building a simple model of the ISS geometry and considering the transport of the primary cosmic radiation field through it. This work is not detailed in the current paper, being instead described in a companion article in this journal (Eakins *et a*l, 2026). Since the conclusion of the HAMLET project the scientific knowledge and state-of-the-art in space dosimetry have progressed. More recent calculations, by the German Aerospace Centre (DLR), to determine the primary radiation field incident on the ISS (Matthiä *et al*, 2013), and then using a slightly different ISS model geometry and a contemporary Monte Carlo code, have yielded alternative datasets for the neutron and light ion particle spectra inside the ISS. These developments are also discussed in the companion paper (Eakins *et al*, 2026). In the present work, however, both the original and alternative particle spectra datasets are considered, and form different respective starting points for the determination of the dosemeter response, which ultimately leads to the estimates of the MATROSHKA neutron doses.

Dosimetry methods used in this report derive from extending the processing regime already in use at UKHSA to the ISS environment, applying substantive correction factors. Other techniques are available (NCRP, 2002), (ICRP, 2013) for estimating doses in LEO environment, and the UKHSA method is not necessarily superior to those other techniques. In terms of the remit to supply a purely neutron dose estimate, the UKHSA method provided this, but should be used comparatively alongside other techniques which may have equal or greater merit.

2 ISS RADIATION ENVIRONMENT

2.1 Field Characterization

There is no single method that can be applied to identify all non-neutron generated tracks on the UKHSA dosemeter. This is because the various components of the radiation field within the ISS cover a very wide energy range and a large number of particle species, so will interact with the dosemeter and its surroundings differently, and will hence demand different techniques to be employed to determine their relative contributions to the signal on the PADC detector. To that end, in attempting to account for the unwanted signal, it is useful to categorize the interactions of the radiation field into the following broad groups:

- Interactions of neutrons with the nuclei in the dosemeter (holder and detector) and astronaut's body that generate nuclear matter. These particles will be mostly recoil protons as well as recoil carbon, nitrogen and oxygen nuclei. There will also be some other light charged particles generated by nuclear reactions on carbon, oxygen and nitrogen, in particular deuterons, tritons, helions and α-particles. Additionally, there will be some capture reactions, such as ^{14}N(n, p), although these only have significant cross sections for low energies and are hence not important in cosmic radiation fields.
- Direct ionization caused by charged particles incident on the dosemeter. If the particle has $\mathrm{LET}_{\infty,\,\mathrm{PADC}}$ > ~40-60 keV μm^{-1} within the entire ~0.6 μm layer removed from the PADC element during the etch process, and if its trajectory makes an angle with the normal to the dosemeter surface that is less than the critical angle for etching (calculated for protons and measured for helium nuclei to be ~60° relative to the normal), then it will be able to produce pits.
- Interactions of charged particles with the nuclei in the detector or holder.

To evaluate the impact of the above components, it is necessary first to characterize the ISS field to determine their relative magnitudes. The neutron and light-ion fluence-energy distributions relevant to the ISS were derived via Monte Carlo modelling (Eakins *et al*, 2026). The first stage of the Monte Carlo modelling process was to generate a neutron fluence-energy distribution that represents the one encountered inside the ISS. To do this, the general-purpose radiation transport code MCNPX 2.6.0 (Pelowitz, 2008) was used to transport the most abundant incident galactic cosmic radiation (GCR) ions and trapped belt ions (H, He, C, O) through a highly simplified model of the ISS hull (Hager *et al*, 2011), namely a slab of aluminium-alloy of thickness 20 g cm^{-2}. The H, He, C, O primary field ion energy distributions were generated using the CREME96 package (Tylka, 1997). The particles that emerged from behind the shield were counted, with interest particularly focussed on the fluence-energy distributions of secondary field neutrons and p, d, t, ^{3}He ions and alphas. Fig. 2 shows the neutron and light ion fluence rates for all light ion species up to and including ^{4}He. Ions heavier than ^{4}He were not calculated because they can be directly measured from the dosemeter (as discussed later), whereas light ions cannot be.

In addition to the above characterization, a further categorization of the radiation field is useful in the current work to describe and analyse the various contributions to the response of the PADC dosemeter. In the following discussions, 'primary particle field' refers to the particle field that is incident on the ISS structure. This is the field outputted by the software package CREME96 (Tylka *et al*, 1997), as discussed further elsewhere (Eakins *et al*, 2026). The 'secondary particle field' is the particle field inside the ISS, incident on the dosemeter and astronaut; it is effectively the output from MCNPX, obtained by transporting the primary field through the ISS hull. The 'tertiary particle field' is the particle field within the etched volume of the detector. Obviously, it is components of the tertiary field that are being measured by the PADC, whilst it is components of the secondary field that are of most relevance in determining the risk to the astronaut. Optimally, of course, assessment of the former by the dosemeter provides good insight into the latter.

The field characterisation as described above was performed during the 2011 HAMLET project. Since then, more recent modelling has been performed to determine the radiation field, yielding revised datasets for particle spectra inside the ISS (Eakins *et al*, 2026). This has allowed the original MATROSHKA data sets to be re-worked using these updated spectra as their starting point. The results from both sets of analyses will be shown later.

2.2 Implications for the PADC dosemeter

The tertiary field will contain particles from many sources, but the ones that are of most interest in terms of the neutron assessment are the recoils from neutron interactions. Charged particles present in the secondary field, which then subsequently traverse the materials of the dosemeter or astronaut to reach the etched volume of the detector, will become part of the tertiary field. However, because these charged particles have not been generated by neutron interactions with the astronaut or dosemeter, they are not wanted in the assessment of neutron dose and therefore need to be accounted for; a large part of this paper is devoted to discussing methods to subtract their contribution.

Protons have the highest fluence of the nuclei incident on the ISS, causing a particular problem for neutron dosimetry because a large number of the neutron-induced pits in the dosemeter are from recoil protons generated by neutron-hydrogen elastic scattering events. It is not possible to determine whether a specific proton-induced pit was due to a recoil proton from a neutron interaction, or a proton that had moved from the secondary field to the tertiary field. For the analysis in this paper the secondary field protons are hence further sub-divided into two components: those that were incident on the front of the dosemeter and those that were incident on the astronaut. A different, but related, correction is required for each component.

The pits in the dosemeter due to tertiary field protons can be split into two different types: proton pits due to the electronic component of stopping ('ECS proton pits') and those due to the nuclear component of stopping ('NCS proton pits'). In addition to the problems associated with the neutron calibration being applied for ECS proton pits, there is an additional problem with double counting when the UKHSA dosemeter is used in combination with other dosimetry systems, since this component of the field may be estimated by the other dosimetry system. Consequently, the neutron and total dose to the astronaut would be overestimated if there is no correction for double counting.

The situation is somewhat different for the NCS proton pits. These are "neutron-like" in that the recoil charged particles will tend to deposit their energy relatively locally, and the average quality factor for the recoils will be comparable to that for recoils from neutrons. The neutron calibration for the dosemeter has had to be used for these events; because they cannot be distinguished from neutron-induced events they will be included in the neutron dose assessment. The assessment given by UKHSA is hence the combined dose from neutrons and the neutron-like interactions of protons.

Helium nuclei, which are the ions that are incident on the ISS with the second highest fluence, also need to be accounted for and the pits they produce subtracted from the total. The fluence of primary field helium nuclei is much lower than that of primary field protons, but they have higher LET at a given energy, so they are intrinsically more detectable.

Further subtractions are performed to account for particles with $Z\geq3$. However, for these ions it was not necessary to produce fluence-energy distributions, because such particles can be identified and accounted for directly by using a secondary chemical etch method, as described in the next section.

3 METHOD

In the following sections the neutron and non-neutron components of the response are isolated from the overall signal on the dosemeter. It is not intended that directly ionizing particles should be measured by the UKHSA dosemeter, so this component is corrected for. The formulae shown in the following sections are used to determine the adjustments applied to the pit counts on the detectors to correct for the unwanted signal from ions. The parameters N_x and C_x are used respectively to denote the measured and calculated number of pits due to particles of type x. In this treatment the N_x values are absolute, and relate to the number of pits actually on the dosemeters. Conversely, the C_x values are relative, since they derive from energy distributions calculated by the Monte Carlo modelling. Systematic uncertainties in the calculated C_x values are not a problem because, ultimately, these values are only used to determine the fractions of the pits caused by particles with Z=0, 1 or 2 relative to the total, as shown later.

The method proceeds in four steps:

1. Measure the total number of electrochemically etched pits on the dosemeter, N_{Total}
2. Measure the number of pits on the dosemeter, $N_{Z\geq3}$, from particles with $Z\geq3$
3. Infer the number of measured pits from particles with $Z<3$, $N_{Z<3}$
4. Decompose $N_{Z<3}$ into its contributions from different particle types, by calculating the expected number of pits from each species, C_Z for Z=0, 1 and 2, relative to their sum, $C_{Z<3}$.

These four steps are discussed in turn.

3.1 STEP 1 – Determination of N_{Total}

In the following section the term 'poncho dosemeters' refers to radiation dosemeters sewn into a waistcoat type jacket 'worn' by the MATROSHKA anthropomorphic upper torso phantom (Reitz, *et al* , 2009).

The raw pit count on a dosemeter is corrected for dose linearity and background signal, giving N_{Total}. At high dosemeter signal levels, equating to neutron doses above a few millisieverts, as typically seen with extended exposures on the ISS, the pits on the dosemeter become increasingly likely to overlap each other, causing under-reading and a non-linear dose response. The dose linearity correction compensates for this. The background correction discounts pits that are due to the intrinsic background signal on the dosemeter and the small increase in natural background signal that arises during issue and/or from transit. It also accounts for the signal accumulated in LEO outwith the actual experimental phase period. The latter part arises because a portion of the signal on the poncho dosemeters was accrued when the dosemeters were in storage in low earth orbit inside the ISS but not attached to the phantom, namely before the dosemeters were installed on the phantom and after the dosemeters were removed and awaiting return to Earth. Technically, these periods were not part of the measurement phase being assessed because the phase began only when the dosemeters were mounted on the phantom and ended when they were dismounted from the phantom. Because of this, a subtraction correction was applied to the poncho dosemeters mean pit count to remove the signal accrued during these periods. The correction was determined from the reference dosemeter pit counts, scaled according to the duration the poncho dosemeters were stored with them, prior to and after the experimental phase. The experimental phase durations were 539 days, 336 days and 404 days respectively for MTR-1, MTR-2A and MTR-2B. The corresponding off-phase storage durations were 81 days, 27 days and 11 days respectively for MTR-1, MTR-2A and MTR-2B (Berger *et al*, 2013). The values for N_{Total} shown in the tables below include all of the above corrections.

3.2 STEP 2 – Determination of $N_{Z\geq3}$

High energy particles with $Z\geq3$ can pass through the detector and could produce pits on both surfaces of the PADC element via direct ionization. Those ions can therefore be distinguished using that signature. Fig. 3 shows ion range data from SRIM (Ziegler *et a*l, 2008), where $E_{\max}$ is the energy above which the LET is too low for the particle to generate pits via direct ionization; the plotted uncertainties show the range for the $\mathrm{LET}_{\infty,\ \mathrm{PADC}}$ threshold taking values of 40 and 60 keV μm^{-1}. The thickness of the dosemeter is 500 μm; multiples, *x*, of this thickness are marked as horizontal lines, which demonstrates that heavier ions are detectable over a greater range in PADC. The particles that cannot produce pits on both surfaces of the PADC element are in the bottom part of Fig. 3: these only achieve sufficiently high LET to induce a pit when they are near the end of their path, at which stage they have too little energy to traverse the 500 μm detector element. The particles in the upper part can maintain the required LET across the whole detector; however, as electrochemical etching only etches one face, the effect of this would not normally be seen. A second, purely chemical etch is therefore performed on both faces of the detector to reveal these pits. The chemical etch produces cone-shaped features where particles with sufficient LET have passed. Pairing the cones on both surfaces enables identification and discrimination of the $Z\geq3$ particle pits, with their summation giving $N_{Z\geq3}$.

The Fig. 3 inset shows a microscope view of the conical pits produced by chemical etching, and the large, rounded, electrochemically etched pits. To establish that the electrochemically etched pit at the top of the left-hand image is due to a $Z\geq3$ particle, the chemically etched cone emerging from it has its axis direction followed whilst focussing through to the other side of the detector. It is seen (*right hand image*) that there is a matching cone on the other side, proving that the particle has completely traversed the detector, and therefore must be a $Z\geq3$ particle.

Reliable identification of the relevant cones depends on the total pit density, field of view of the microscope, clarity of the detector material, etc. Long periods on the ISS, as pertained during the Matroshka phases and that also often apply to astronaut missions, typically exceed 1500 counted pits, which is the level beyond which this method is not viable due to difficulty in reliably locating matching cones against the high density electrochemical etched pit background. Instead, an average $Z\geq3$ daily pit rate is used in such cases to imply the value of $N_{Z\geq3}$. This average has been obtained from the evaluation of dosemeters from a number of short astronaut missions on the ISS. Based on all available data, the current mean of 4.72 (±1.03) pits per day are expected from $Z\geq3$ particles.

Because the $Z\geq3$ particle contribution is based on direct measurement, their subtraction is more precise and independent of the neutron signal than for the other charged particle species.

3.3 STEP 3 – Determination of $N_{Z<3,M}$

Subtraction of the number of pits caused by $Z\geq3$ particles, $N_{Z\geq3}$, from the total number of pits on the dosemeter, N_{Total}, leaves the number of pits caused by $Z<3$ particles:

$$N_{Z<3} = N_{Total} - N_{Z\geq3} \qquad \text{Eq. (1)}$$

The parameter $N_{Z<3}$ contains components from neutrons (Z=0), hydrogen isotopes (Z=1), and helium isotopes (Z=2). Resolution of a given component, N_z, and specifically the neutron component ($N_{Z=0}$), is obtained from the ratio:

$$N_Z = \left(\frac{C_Z}{C_{Z<3}}\right) N_{Z<3} \qquad \text{Eq. (2)}$$

where C_Z is the expected number of pits from particles of type Z calculated by MCNP and analytic methods, and the parameter $C_{Z<3}$ is derived by summing the number of expected pits calculated for Z = 0, 1 and 2 species:

$$C_{Z<3} = C_{Z=0} + C_{Z=1} + C_{Z=2} \qquad \text{Eq. (3)}$$

as shown in the next step.

3.4 STEP 4 – Determination of $C_{Z<3}$

3.4.1 $C_{Z=0}$

The calculated neutron contribution, $C_{Z=0}$, is obtained by folding the neutron fluence-energy response function of the dosemeter with an appropriate neutron energy distribution. For the HAMLET project, a determined Monte Carlo neutron energy distribution was used for the ISS (Eakins, 2026), Fig. 4.

The total integrated fluence rate for the energy distribution is also determined in the Monte Carlo calculations. This total is multiplied by the folded fluence response of the dosemeter for that distribution, to give the calculated neutron pit rate. Finally, this value is multiplied by the duration of the mission to give the expected number of neutron pits on the detector, $C_{Z=0}$, relative to the presumed Monte Carlo normalization.

Since the original evaluation of the MATROSHKA data during the HAMLET project, the authors have had access to more recent modelling data derived by DLR (Matthiä *et al*, 2013, Eakins, 2026). The impact of these modelling data on the neutron pit rate is discussed later.

3.4.2 $C_{Z=1}$ and $C_{Z=2}$

There is no detailed measured fluence-energy response function for the UKHSA dosemeter for hydrogen or helium ions. So, even though corresponding spectra for inside and outside the ISS are available, their contribution to the dosemeter signal cannot be obtained by the folding technique described in Section 3.4.1 for neutrons. Also, and as mentioned earlier, the ranges for which their LET reaches the threshold for producing pits is much less than the 500 μm thickness of the dosemeter, so they cannot produce pits on both faces and the secondary chemical etch method described for $Z\geq3$ ions is therefore not usable. Instead their contribution is calculated using an analytical method based on experimentally determined $\mathrm{LET}_{\infty,\ \mathrm{PADC}}$ thresholds combined with Monte Carlo calculations of the charged particle spectra inside the ISS.

To determine the LET thresholds, calibrations to protons and ^{4}He ions were performed at the Heavy Ion Medical Accelerator, HIMAC, Chiba, Japan (Bartlett *et al.*, 2003; Uchihori *et al.*, 2007, 2010). The experiment was performed for normally incident 40 MeV and 70 MeV protons, and 576 MeV ^{4}He ions, at 0°, 40°, 50° and 60° incidence. The following description of those measurements focuses on the proton evaluation, but the same techniques apply to ^{4}He ions. Stacks of detectors were arranged (Fig. 5) that were thick enough such that the ions stop within them. For 40 MeV and 70 MeV protons, their range variation was observed to be 1.2 mm and 2.8 mm, respectively, at the 95% confidence level. This range variation is several multiples of the detector thickness, guaranteeing that the Bragg peaks for some of the ions will coincide with a detector surface on a few of the detectors within the stack, and pits will be recorded on those where the LET threshold for detection is exceeded. The lower the LET threshold, the greater the proportion of the ion's Bragg peak/curve width that can contribute to the signal on the detector, and the ion will hence be detectable over a greater range. The results for 40 MeV and 70 MeV protons are plotted together in Fig. 5. As expected, the figure shows that most of the recorded pits are distributed at distances that are tightly around the mean ranges for the two incident proton energies used. Analogous results were found for the helium ions, but for brevity are not included here.

The critical range, R_{crit}, i.e. the etchable track length (where the LET threshold for detection is exceeded) of the proton in PADC, can be determined by comparing the number of pits counted in the distribution, Fig. 5, with the applied fluence, using the method shown in Fig. 6. For example, if the etchable track length were exactly equal to one detector thickness then a given proton will be etchable at one, but only one, of the detector faces. Hence each proton would create one pit count at some point in the stack, but on one detector only, and the summation of all such pit counts (N in Fig. 6) on all the detectors would then exactly equal the applied fluence. In reality though the etchable length is much less than a detector thickness, meaning the likelihood of the proton track being above the LET threshold for detection when it crosses one of the etched surfaces will be low. So, most of the protons go un-detected, leaving only those few protons that had their Bragg peak roughly coincident with the detector surface contributing to the measured signal, albeit they must still exceed the LET threshold for detection. Hence the counted pits, N, are normally much less than the applied fluence, Φ, and the etchable track length, R_{crit}, is therefore much less than the detector thickness. The critical range is converted to a proton energy and an LET value using range-energy data from SRIM (Ziegler *et al*, 2008). This value is interpreted as the LET threshold of detection.

From the 40 MeV and 70 MeV exposures, the HIMAC calibrations gave a mean proton $\mathrm{LET}_{\infty,\ \mathrm{PADC}}$ threshold for normal incidence of 44 keV $\mu\mathrm{m}^{-1}$ (Fig. 6). For helium nuclei at normal incidence the threshold was measured as 58 keV $\mu\mathrm{m}^{-1}$.

The proton threshold equates to approximately 600 keV. The lowest fast neutron energy that can be measured by the UKHSA dosemeter is approximately 50 keV, as seen in Fig. 7, which shows fluence response at nominal energies of 70 keV and 100 keV measured at the UK's National Physical Laboratory (NPL). The nominal energies apply to the centre of the two phantom front faces, but because multiple dosemeters were positioned across each phantom face and the energy is changing rapidly with angle, this allowed an approximate assessment of the fluence response down to about 50 keV, based on the dosemeters mounted on the phantom exposed to a nominal 70 keV field. At about 50 keV the fluence response is observed to almost drop to zero. Because detection of a 50 keV neutron will likely be due to a single proton recoil event, it may be inferred that the minimum detectable proton energy is also about 50 keV. A 50 keV proton has a range in PADC of 0.64 μm, which is approximately the thickness of PADC removed during the etching process.

It follows that all normally incident protons traversing the etched surface of the PADC will produce pits if their energies, E_{p}, are such that $\sim 50\ \mathrm{keV} \leq E_{\mathrm{p}} \leq \sim 600\ \mathrm{keV}$. It should be noted that these values relate to electrochemical etching, so other laboratories that use chemical etching will derive different values.

Within the etched layer of the PADC dosemeter, a proton's ability to form a pit is independent of its origin. However, those that were not produced as recoils from neutron interactions within the phantom or astronaut or dosemeter need to be excluded from the neutron dose assessment to avoid an over-estimate. This is particularly important because such protons, i.e. those that were incident on the phantom/astronaut/dosemeter, carry a much lower detriment per unit absorbed dose than those produced in the neutron interactions, as reflected by their lower radiation weighting factor (ICRP, 2007). A description of the analytical method used to determine the proton contribution now follows.

A simple model (Fig. 8) of the dosemeter mounted on the surface of an ICRU four-element tissue equivalent (30 cm diameter) sphere was used to estimate the fraction of the secondary field protons that will produce pits in the dosemeter via the electronic component of their stopping. The figure shows how the path length of protons through matter is calculated for irradiation from the front (through the dosemeter), or from the back (through the ICRU 4 element tissue equivalent sphere).

Pits on the detector are produced by protons incident on the rear (etched) surface of the detector if their energy is in the range ~50 keV ≤ E_p ≤ ~600 keV and their angle of incidence is less than the calculated 60° critical angle for detection using the electrochemical (EC) etch. The ICRU sphere is used as an approximation to the human torso, because its symmetry simplifies calculations and it gives a range of chord lengths that reflect the similar range of proton path lengths through the human body or anthropomorphic phantom considering where the dosemeter might be worn, e.g. on the waist or chest. The effect of varying either the tissue thickness from the front or the sphere's diameter is considered later.

The chord length, L, in Fig. 8 is defined as the thickness of tissue equivalent material that the incident protons pass through to get to the etched volume of the detector. When incident from the front, this material corresponds to the dosemeter, holder and overlying materials, e.g. Matroshka container or any clothing; the ICRU sphere provides no shielding from particles incident on the dosemeter from the front. When incident from the back, L relates to the ICRU sphere and back of the holder, though the latter may be ignored due to its small size relative to the sphere. The thicknesses of the various materials encountered along L are converted to tissue equivalent thicknesses using their densities relative to the unit density of ICRU 4 element tissue. These thicknesses are then used in conjunction with the LET thresholds to determine the energy interval of incident protons that will be etchable from a given direction. This interval is the range of energies that protons incident from that angle must be within such that, when they have passed through the appropriate mass-thickness of tissue, L, their $\mathrm{LET}_{\infty,\ \mathrm{PADC}}$ normal to the detector plane is ≥ 44 keV μm^{-1} for the entire length of their track through the ~0.6 µm thick volume of PADC removed by the electrochemical etch process. The conversions from distances to energies are achieved using range-energy tables (Ziegler *et al*, 2008).

3.4.2.1 **Criteria for particle latent tracks to form pits**

The analytical method used to derive the etchable proton energy windows is illustrated in Fig. 9 and Fig.10. The procedure can be summarized as follows:

1. Unperturbed particle fluences are incident at point *A* in the figure. Either the MCNPX-calculated energy distributions for inside the ISS are used for those fluences, or the raw CREME spectra for outside the ISS.
2. The phantom and, to a lesser extent, the dosemeter alter the energy distributions of protons passing through them. Consequently, the energy distributions at the detector surface are different from the incident field. The extent of the change may be accounted for by considering the mass-thicknesses of material that a proton passes though.
3. With knowledge of how the PADC detector responds, it is possible to retrospectively calculate the detectable energy interval at point *A* that would lead to a measurable signal.

This process may be explained more thoroughly. The method involves working backwards from knowledge of the energy interval that a proton passing though the etchable volume must be in if it is to form a pit after the detector is etched. This etch criterion is governed by the proton LET: it is assumed that the LET threshold for pit formation must be exceeded over the entire etched volume behind the detector rear face. In other words, the proton LET must be greater than the LET threshold for the entire portion of its track between points *B* and C (Fig. 9 and Fig. 10). For a proton at normal incidence, the experimentally-determined threshold LET for PADC is 44 keV μm^{-1}. Moreover, this LET must be maintained over the ~0.6 µm etched volume thickness of PADC removed by the electrochemical etch process. The LET may be converted to an energy. The issue then becomes: for a given angle, what is the range of energies that a proton at point *A* must have such that, when it has passed though the intervening material, it has residual energy within the limits for maintaining an LET of 44 keV μm^{-1}?

To solve this for a given angle θ, a consideration of the shielding geometry permits an estimate to be made of the equivalent thickness of tissue that particles from that direction traverse through on their way to the etched volume. Using this, and range-energy data (Ziegler *et al*, 2008) based on the continuous slowing down approximation (CSDA), it is possible to calculate the energy E_A that a proton at point *A* must have had if its energy at point *B* is E_B. Repeating this retrodictive approach for the minimum and maximum values of the energy range of interest across the etched volume, the corresponding energy range of an 'eligible' incident proton at *A* can be obtained as a function of angle. Subsequently, repeating for all angles (in appropriate bins) up to the critical angle, from both the front and the rear, provides insight into the overall contribution to the dosemeter signal from the incident proton field.

The above methods are described in more detail elsewhere (Hager *et al*, 2011).

3.4.2.2 **Proton detectable energy windows**

The calculated minimum and maximum energy bounds at point A (Fig. 9 and Fig. 10) define the etchable energy interval that a proton from a given angle of incidence must be in if it is to produce a pit on the detector. A proton within this energy interval is assumed to produce a pit on the detector. Therefore, determining the particle fluence within this energy interval gives the number of pits that will be produced on the detector. The method used to determine the etchable fluence-energy interval, $\delta\Phi$, is specified by Equation 4. The ratio of the etchable energy interval (δE) to the full energy bin width (E) is multiplied by the fluence in the full bin width (Φ), to obtain the proton fluence that will produce pits ($\delta\Phi$). The proton fluence-energy distribution used is either that calculated by Eakins for inside of the ISS (Eakins *et al*, 2026), as shown in Fig. 2, or the raw CREME spectrum for outside of the ISS. This procedure is repeated for all angles of incidence, and the number of protons is summed to estimate the total proton contribution from all angles.

$$\delta\Phi = \frac{\delta E}{E}\Phi \qquad \text{Eq. (4)}$$

The etchable energy interval will vary depending on the angle of incidence and is typically very narrow compared to the full energy bin width; hence, although the incident fluences are high, only a very small proportion of the protons produce pits on the detector. Consequently, it can be shown that the neutron-induced pits are not dominated by pits from incident protons. For a given angle of incidence relative to the normal to the dosemeter plane, the energy window decreases as the thickness traversed increases, so the contribution to the dosemeter signal from protons is much greater for particles incident from the front than from the rear, with a ratio of approximately 7:1 calculated.

3.4.2.3 **Proton critical angle**

The detectable energy windows described above need only be calculated for protons incident at angles less than the proton critical angle for etching. For exposures from the front, this was determined by setting the critical angle as the maximum angle, θ_{Crit}, for which the component of $\mathrm{LET}_{\infty,\,\mathrm{PADC}}$ normal to the dosemeter plane (i.e. $\mathrm{LET}_{\infty,\,\mathrm{PADC}} \times \cos\theta$, where θ is the angle subtended between the normal to the dosemeter plane from the front and the incident proton direction) is ≥ 44 keV $\mu\mathrm{m}^{-1}$ for the entire $0.6/\cos(\theta)$ µm path length through the etched volume of the detector. The proton critical angle is calculated as 60°; no proton of any energy is detectable from angles further from the normal than this. An analogous correction is used for exposures from the rear.

3.4.2.4 ***Z*=2 particles**

The methods described for protons are applied in a similar way to determine the component of the signal on the dosemeter that is caused by helium ions. The measured 58 keV $\mu\mathrm{m}^{-1}$ LET threshold, range-energy data, and calculated fluence-energy distribution for helium ions (Eakins *et al*, 2026), are used.

4 DOSE QUANTITY

During the 2011 HAMLET project, the quantity effective dose was used to report doses, with its values obtained using the dose conversion coefficients from ICRP 74 (ICRP, 1996). The same approach is described in this paper. However, it is noted that the revised conversion coefficients from ICRP 116 (ICRP, 2010) would now be used for this quantity. But in fact choosing the most appropriate quantity for space dosimetry is not straightforward. Astronauts on the ISS are exposed to much more penetrating higher energy radiation than their terrestrial counterparts. Consequently, a component of the dose equivalent is deposited with very high LET. The standard dose quantities that are available do not offer good estimates of the detriment associated with such radiation exposures.

There are concerns about the use of fixed value radiation weighting factors, w_R, and hence effective dose, in cosmic radiation fields. There is hence a general preference amongst those working in radiation exposure in the space environment to use a quality factor, $Q(L)$, based dose quantity. This is driven in part by the observation above that a fixed value for w_R, for all particles other than neutrons, is inappropriate in cosmic ray fields, but also by the nature of the instruments available for dose estimation: tissue equivalent proportional counters estimate dose from the lineal energy, a quantity related to the LET, so they are only useful for $Q(L)$ type quantities. This is reflected in ICRP Publication 123 (ICRP, 2013) which concludes that: "The simple concept of considering the differences in radiobiological effectiveness by radiation weighting factors, w_R, (e.g. a constant radiation weighting factor of 20 for all heavy ions of all energies) is not appropriate for dosimetry in space, and the quality factor, Q, is applied for the definition of the quantity dose equivalent in an organ or tissue of the human body."

Effective dose equivalent, H_E, originally defined in ICRP Publication 26 (ICRP, 1977) and now recommended in ICRP Publication 123 (ICRP, 2013), has therefore been used in more recent measurements since the HAMLET project. Whilst effective dose equivalent may be the preferred quantity, personal dose equivalent could also be used to ensure that the most conservative estimate of neutron dose is obtained. Effective doses could also potentially be used for comparative analyses, albeit with caveats. Typically, UKHSA routinely reports astronaut doses using each of these quantities, with their respective conversion coefficients used in place of those exemplified in Section 5.

Comprehensive datasets of conversion coefficients do not exist for all dose quantities. For example, $H_p(10, \mathrm{ISO})$ per fluence conversion coefficients were based on available data calculated (Tanner, 2008) up to 20 MeV, but because those data do not cover the whole energy range of interest for the ISS fields, they were further extended to 10 TeV by fixing their ratio relative to E_{ISO}, for which higher energy data are available (ICRP, 2010). Specifically, the relationship $H_p(10, \mathrm{ISO})=1.296\times E_{\mathrm{ISO}}$ is applied for these higher energies, where 1.296 is the ratio between the quantities at 20 MeV. Although clearly not perfect, it is suggested that this approach provides a suitable pragmatic solution to the use of this quantity, given the lack of available data and the overall large uncertainty budget associated with the physical dosimetry.

In the future, potential replacement of $H_p(d,\theta)$ with the newer quantity, personal dose, H_p, as recommended in ICRU Report 95 (ICRU, 2020), would change the situation greatly, because it will no longer be the quantity giving the highest dose estimate, as shown later.

5 NEUTRON DOSE

The final neutron effective dose estimate is obtained as follows. The PADC sheet from which the dosemeter was taken has its personal dose equivalent response, $R_{Hp(10,0),\mathrm{AmBe,Meas}}$, measured by exposing it at normal incidence to the ^{241}Am-Be calibration source within UKHSA's Secondary Standards metrology laboratory. Similarly, the calculated dose equivalent response of the dosemeter to ^{241}Am-Be, $R_{Hp(10,0),\mathrm{\ AmBe,\ Calc}}$, is also determined by folding the dosemeter fluence response function with the ^{241}Am-Be neutron energy distribution, and dividing the result by the outcome of folding the $H_p(10,0°)$ fluence to dose conversion coefficients with the same energy distribution. The calculated response of the dosemeter to the neutron field inside the ISS, in terms of effective dose, $R_{E(\mathrm{ISO}),\mathrm{ISS,\ Calc}}$, is also determined in the same way, but using the energy distribution of Eakins (MCNPX v2.7.0), shown in Fig. 4 and the dosemeter isotropic fluence response function and effective dose isotropic conversion coefficients (ICRP 74, 1996). It follows that the dose response characteristic of the dosemeter in the neutron field inside the ISS, corrected for the measured response to the calibration source, $R_{E(\mathrm{ISO}),\mathrm{\ ISS}}$, is obtained from Equation 5:

$$R_{E(\mathrm{ISO}),\mathrm{ISS}} = R_{E(\mathrm{ISO}),\mathrm{ISS,C}} * \frac{R_{H_{p}(10,0),\mathrm{AmBe,M}}}{R_{H_{p}(10,0),\mathrm{AmBe,C}}} \qquad \text{Eq. (5)}$$

where the subscripts C and M refer to calculated (by folding) and measured values.

The above approach corrects for systematic variations in the dosemeter neutron response from one measurement to another due to different sheets of PADC being used, with the assumption that differences in the measured ^{241}Am-Be calibration dose response are matched by the same differences in dose response to the neutron field inside the ISS.
This normalization is a relatively new approach for UKHSA that is applied to all recent measurements. However, it was not actually applied to the MATROSHKA data during the 2011 HAMLET project. The effect of applying the more recent approach to the MATROSHKA data is discussed later in Section 8. Instead, during the HAMLET project, the dose response characteristic of the dosemeter in the neutron field inside the ISS was just the calculated value obtained from folding.

The last step in determining the neutron dose is to divide the neutron pits, $N_{Z=0}$, obtained using Equation 2, by the neutron dose response characteristic of the dosemeter in the neutron field in the ISS, to obtain the estimate of the neutron effective dose for isotropic irradiation E_n(ISO):

$$\text{Neutron } E_{\mathrm{n}}(\mathrm{ISO}) = \frac{N_{Z=0}}{R_{E(\mathrm{ISO}),\mathrm{ISS}}} \qquad \text{Eq. (6)}$$

6 RESULTS: MATROSKHA 2B

The MATROSHKA neutron PADC measurements were made with dosemeters placed on the poncho jackets 'worn' by the MATROSHKA phantom during the exposures. The value for the measured pits on the detector, N_{Total}, used below correspond to the ESA-MATROSHKA project mean pit counts for phase 2B. All values in parentheses show one standard uncertainty, which is derived as discussed in Appendix A. In a more general sense, however, the following analysis acts as a worked example that illustrates the neutron dosimetry procedures described in Sections 3 to 5, and demonstrates the flow of information through the method.

Table 2 shows the calculated neutron pit accrual rate on the dosemeter, as obtained using the method in Section 3.4.1 and determined for the neutron energy distribution for inside the ISS based on CRÈME + MCNP modelling.

Table 2
Calculated neutron pit rate based on the dosemeter's calculated fluence response in the neutron energy distribution inside the ISS and the total neutron fluence rate obtained from the MCNP modelling

Neutron energy distribution	Total neutron fluence rate ($\mathrm{cm^{-2}\ s^{-1}}$)	Fluence response ($10^{-6}\ \mathrm{cm^2}$)	Pit rate ($10^{-5}\ \mathrm{s^{-1}}$)
CRÈME + MCNP[a]	1.255	37.3	4.68 (0.41)

a Source: Eakins, 2026

Bracketed values are 1 standard uncertainty

The neutron pit accrual rate from Table 2 is multiplied by the total duration of the exposure to give the calculated pits on the dosemeter from neutrons, as shown in Table 3.

Table 3

Calculated neutron pits on detector, $C_{Z=0}$

Calculated neutron pit rate (d^{-1})	**Exposure duration (d)**	**Calculated neutron pits on detector $C_{Z=0}$**
4.04 (0.36)	404	1634 (144)

Bracketed values are 1 standard uncertainty

Table 4 shows the number of pits on the detector from ions. $Z \geq 3$ particles are listed separately, as they are based on measured data as detailed in Section 3.2, whereas the results for $Z=1$ and $Z=2$ particles are values calculated from the combination of Monte Carlo and analytical methods described in Section 3.4.2. The daily pit rates from $Z=1$ and $Z=2$ interactions are those based on the particle spectra output from the Monte Carlo modelling (Eakins *et al*, 2026).

Table 4

Charged particle pits on detector, measured for $Z \geq 3$, calculated for $Z=1$ and $Z=2$

Particle type	**Pit rate (d^{-1})**	**Exposure duration (d)**	**Pits on detector**
$Z \geq 3$	4.3 (1.0)	404	1737 (404)
$Z=1$	1.58 (0.46)	404	638 (186)
$Z=2$	0.027 (0.024)	404	11 (10)

Bracketed values are 1 standard uncertainty

The measured $Z \geq 3$ pits obtained from Table 4 are subtracted from the total measured pits on the dosemeter to give the measured number of $Z<3$ pits on the dosemeter (Equation 1) as shown in Table 5.

Table 5

Measured pits on the detector, with $N_{Z<3}$ assumed to be the difference between the total pits and $Z \geq 3$ pits

N_{Total}[a]	$N_{Z \geq 3}$[b]	$N_{Z<3}$[c]
8047 (1229)	1737 (404)	6309 (1306)

a total net pits after linearity and background correction

b measured pits from $Z \geq 3$ particles

c estimated pits left from $Z<3$ particles

Bracketed values are 1 standard uncertainty

The above value for N_{Total} is the mean number of pits on the dosemeters on the poncho for the MATROSHKA 2B phase, corrected for linearity, and background. The calculated values for $Z=0$ (neutron), $Z=1$, and $Z=2$ pits, obtained from Tables 3 and 4, are shown in Table 6. When added they give the calculated sum for $Z<3$ pits, $C_{Z<3}$, as described in Equation 3. In Table 6, the first column gives the measured $Z<3$ pits, $N_{Z<3}$, which is significantly higher than the calculated sum. This is not a problem because in Equation 2 the data are applied as ratios, and are hence self-normalizing, and the calculated values for all particles of $Z<3$ are adjusted to give the correct measured value. This difference between the calculated and measured pits could possibly arise from differences in the shielding present during the MATROSHKA exposure compared to the shielding used in the Monte Carlo model. For example, localised changes to the materials stored close to the MATROSHKA phantom could affect the particle fluences incident on it.

Table 6

Measured vs. calculated pits for $Z<3$ particles, calculated values are based on applying analytical methods to MCNP output

Measured pits	**Calculated pits**			**Calculated sum**
$N_{Z<3}$[a]	$C_{Z=0}$[b]	$C_{Z=1}$[c]	$C_{Z=2}$[d]	$C_{Z<3}$[a]
6309 (1306)	1634 (144)	638 (186)	11 (10)	2283 (235)

a measured or calculated pits from $Z<3$ particles

b calculated pits from $Z=0$ (neutrons)

c calculated pits from $Z=1$ (protons, deuterons, tritons), obtained by method in Section 3

d calculated pits from $Z=2$ (alphas and helions), obtained by method in Section 3

Bracketed values are 1 standard uncertainty

Table 7 shows the values once the corrections to the $Z<3$ pits have been made, along with the total pit count, N_{Total}, and the $Z\geq3$ pits, $N_{Z\geq3}$. Table 7 also contains the final corrected estimated pits for all particle types considered, in particular the final corrected neutron pit counts, $N_{Z=0}$.

Table 7

Measured pits for all particles, with $N_{Z=0}$, $N_{Z=1}$, $N_{Z=2}$ being estimates of the true number of pits once corrections to the $Z<3$ pits have been made

N_{Total}[a]	$N_{Z\geq3}$[b]	$N_{Z=0}$[c]	$N_{Z=1}$[d]	$N_{Z=2}$[e]
8047 (1229)	1737 (404)	4515 (1016)	1764 (546)	30 (24)

[a] measured total pits after linearity and background correction

[b] measured pits from $Z\geq3$ particles

[c] corrected pits from $Z=0$ (neutrons)

[d] corrected pits from $Z=1$ (protons, deuterons, tritons)

[e] corrected pits from $Z=2$ (alphas, helions)

Bracketed values are 1 standard uncertainty

The result for $N_{Z=0}$ is divided by the dosemeter response characteristic (Equation 5), to give the estimated neutron dose (Equation 6). Table 8 shows how the dose response characteristic is obtained from the determined neutron energy distribution derived using CRÈME and MCNP.

Table 8
E(ISO) response characteristic, based on folding the neutron energy distribution with both the dosemeter fluence-energy response function and effective dose conversion coefficients and dividing the former by the latter

Neutron energy distribution	**E(ISO)/Φ[a] (pSv cm^2)**	**$R_{\Phi \mathrm{ISO}}$[b] (10^{-6} cm^2)**	**$R[E$(ISO)$]$[c] (mSv^{-1})**
CRÈME + MCNP	366	37.3	102 (8)[d]

a E(ISO) fluence to dose conversion coefficient using ICRP 74 data
b isotropic fluence response of the dosemeter
c E(ISO) integral dose response characteristic of dosemeter
d half-range using R_{Φ} envelope of ± 1 standard uncertainty

Bracketed values are 1 standard uncertainty

Lastly, the corrected neutron pits are divided by the dose response characteristic (Equation 6), to yield the final neutron dose, as shown in Table 9.

Table 9
Determination of neutron E(ISO), from the measured neutron pits and the calculated number of pits per neutron effective dose

Neutron energy distribution	**$N_{Z=0}$[a]**	**$R[E$(ISO)$]$[b] (mSv^{-1})**	**E(ISO)[c] (mSv)**
CRÈME + MCNP [d]	4515 (1016)	102 (8)	44 (11)[e]

a corrected pits from Z=0 (neutrons)
b E(ISO) integral dose response characteristic of dosemeter
c Assessed E(ISO)
d Neutron energy distribution derived using CRÈME and MCNP
e combined standard uncertainty: on integral dose response characteristic; Z≥3, Z=1, Z=2 particle subtractions; and random uncertainty on pit counting.

Bracketed values are 1 standard uncertainty

A basic sensitivity analysis was also performed to assess how variations in tissue covering thickness and LET threshold might impact the assessment, this is detailed in Appendix B.

7 SUMMARY OF MATROSHKA NEUTRON DOSE RESULTS

The MATROSHKA neutron PADC measurements were made with dosemeters placed on the poncho jackets 'worn' by the MATROSHKA phantom during the exposures. Table 9 and Table 10 summarize the neutron dose evaluation, using the mean pit counts to determine $N_{Z=0}$ and E(ISO). The mean value in each MATROSHKA phase encompasses all results from dosemeters on the front and back of the poncho, and is hence the best option for assessing effective dose, assuming isotropic exposure. The results are based on the original modelling work performed during the HAMLET project. See Appendix C for dosemeter pit counts for all locations on the poncho jackets.

MTR-2B orbit parameters and the relevant solar cycle period were used to obtain the CREME96 primary particle spectra for the MTR-2B calculations. However, exactly the same primary particle spectra were also used for the MTR-2A calculations, even though it took place during a different part of the solar cycle. This approximation for MTR-2A was made due to the very limited computational resources at the time of HAMLET, which didn't allow time to perform a separate calculation using MTR-2A's actual orbit parameters and period of the solar cycle. Some limited discussion of the effects of solar cycle period on the primary particle spectra are discussed in a companion article in this journal (Eakins *et al*, 2026).

Table 10
Measured pits for all particles for MTR-1, MTR-2A, MTR-2B

MATROSHKA phase	N_{Total}[a]	$N_{Z\geq3}$[b]	$N_{Z=0}$[c]	$N_{Z=1}$[d]	$N_{Z=2}$[e]
MTR-1	18421 (2952)	2318 (539)	3181 (2367)	12895 (4137)	28 (35)
MTR-2A	8665 (1407)	1445 (336)	5167 (1125)	2019 (615)	34 (27)
MTR-2B	8047 (1229)	1737 (404)	4515 (1016)	1764 (546)	30 (24)

a measured total pits after linearity and background correction

b measured pits from $Z\geq3$ particles

c corrected pits from $Z=0$ (neutrons)

d corrected pits from $Z=1$ (protons, deuterons, tritons)

e corrected pits from $Z=2$ (alphas, helions)

Table 11

Determination of E(ISO) for MTR-1, MTR-2A, MTR-2B

MTR phase	$N_{Z=0}$[a]	**$R[E$(ISO)]**[b] **(mSv^{-1})**	**E(ISO)**[c] **(mSv)**	**E(ISO)**[c] **(µSv d^{-1})**
MTR-1	3181 (2367)	102 (8)	31 (23)[d]	58 (43)[d]
MTR-2A	5167 (1125)	102 (8)	51 (12)[d]	151 (35)[d]
MTR-2B	4515 (1016)	102 (8)	44 (11)[d]	110 (26)[d]

a corrected pits from $Z=0$ (neutrons)

b E(ISO) integral dose response characteristic of dosemeter

c Assessed total E(ISO) and E(ISO) per day

d combined standard uncertainty: on integral dose response characteristic; $Z\geq3$, $Z=1$, $Z=2$ particle subtractions; and random uncertainty on pit counting

The uncertainty of 74 % on the neutron dose assessment for the MTR-1 phase is higher than the other two phases. This is largely because outside of the ISS the signal on the dosemeter is dominated by protons, and because the neutron dose depends on the correction for the proton subtraction, this makes the neutron dose uncertainty large. Even this quoted uncertainty may be an underestimate, however, because the $Z\geq3$ component is not accurately known for that phase.

For the evaluation of the MATROSHKA data performed during the HAMLET project, the integral dose response characteristic for the neutron field in the ISS, $R_{E(\text{ISO})}$, was calculated by folding the dosemeter fluence response function with the relevant neutron fields, similarly folding the effective dose conversion coefficients with the relevant neutron fields, and dividing the result of the former by the result of the latter. This approach assumes that the fluence response function remains constant over time. However, it can be affected by factors such as PADC manufacturing variations and sheet thickness, so the use of a fixed fluence response function may not always best represent the response for individual sheets. Subsequent to the HAMLET project it was therefore decided to apply a normalisation, or correction factor, based on a standard ^{241}Am-Be $H_{\text{p}}(10)$ sheet calibration sensitivity measurement. Any difference between this measured sensitivity and the calculated (folded) sensitivity to the same radionuclide is applied as a correction factor to the calculated effective dose response characteristic for the ISS neutron field (Equation 5). The resulting correction factors, and the effect of their application, are shown in Table 12 for the three MATROSHKA phases.

Table 12

^{241}Am-Be correction factors for MTR-1, MTR-2A, MTR-2B

MTR phase	**^{241}Am-Be correction factor**[a]	**E(ISO) un-corrected**[b] **(mSv)**	**E(ISO) corrected**[c] **(mSv)**	**Diff**[d] **%**
MTR-1	0.8364	31	37	+20 %
MTR-2A	0.9707	51	53	+3 %
MTR-2B	1.1809	44	37	-15 %

a ratio of measured to calculated ^{241}Am-Be sensitivity
b *E*(ISO) without application of ^{241}Am-Be correction factor
c *E*(ISO) with application of ^{241}Am-Be correction factor
d Change in assessed *E*(ISO) from applying the ^{241}Am-Be correction factor

The efficacy of applying this correction is dependent on the sensitivity of a PADC sheet to both ^{241}Am-Be and the ISS neutron fields being consistent with each other. So for example, if the ^{241}Am-Be sensitivity of a given sheet is found to be high, then it is assumed that its sensitivity in the ISS neutron field would also be high.

As previously mentioned, choosing the most appropriate dose quantity for space dosimetry is not straightforward. Currently, *effective dose equivalent*, H_E, may be considered to be the most appropriate quantity. The choice of dose quantity can have a significant effect on the magnitude of the reported neutron dose. This is illustrated in Table 13, by comparing the results obtained by using a selection of potential dose quantities.

Table 13
Comparison of neutron total doses by dose quantity, for the three Matroshka phases

MTR phase	ICRP 123 H_E(ISO)[a] ICRP 60 $Q(L)$ (mSv)	ICRP 123 H_E(ISO)[b] NASA $Q(Z,E)$[g] (mSv)	ICRP 74 H_p(10,ISO)[c] (mSv)	ICRP 116 E(ISO)[d] (mSv)	ICRP 74 E(ISO)[e] (mSv)
MTR-1	26 (19)[f]	34 (26)[f]	39 (29)[f]	28 (21)[f]	31 (23)[f]
MTR-2A	42 (10)[f]	55 (13)[f]	63 (15)[f]	46 (11)[f]	51 (12)[f]
MTR-2B	36 (9)[f]	48 (12)[f]	55 (14)[f]	40 (10)[f]	44 (11)[f]

[a] assessment using effective dose equivalent, HE(ISO) ICRP 60 Q(L) calibration of 124 (13) counts mSv-1

[b] assessment using effective dose equivalent, HE(ISO) NASA Q(Z,E) calibration of 93 (11) counts mSv-1

[c] assessment using personal dose equivalent, Hp(10, ISO) calibration of 82 (13) counts mSv-1

[d] assessment using effective dose, E(ISO) calibration of 112 (12) counts mSv-1

[e] assessment using effective dose, E(ISO) calibration of 102 (14) counts mSv-1

[f] combined one standard uncertainty: includes uncertainties on integral response characteristic, Z≥3 particle subtraction, Z=1 particle subtraction, Z=2 particle subtraction, and on pit counting.

[g] Q(Z,E), where E is energy

8 COMPARISON OF MATROSHKA 2B NEUTRON DOSES OBTAINED USING CRÈME + MCNP MODELLING RESULTS AND DLR GCR + GEANT4 MODELLING RESULTS

As previously mentioned, since the 2011 HAMLET project, the authors have had made available to them alternative calculations of the particle fields inside the ISS. The alternative datasets result from use of an advanced environmental code, developed at DLR, Germany, to determine the primary particle spectra incident on the ISS during the MATROSHKA 2B phase (Matthiä *et al*, 2013). These primary particle spectra were then used in combination with transport model GEANT4 to give an alternative set of neutron, proton and helium particle spectra for inside the ISS (Eakins *et al*, 2026). The latter have been used as the basis for a re-evaluation of the neutron dose estimate for the MATROSHKA 2B exposure inside the ISS, to compare with the dose estimate using the MCNP modelling adopted in the HAMLET project.

The neutron pit rate based on the alternative modelling (Matthiä *et al*, 2013; Eakins *et al*, 2026) is shown in Table 14, and Table 15 shows the dose response characteristic derived from the alternative modelling. These data are used in the full comparison which is given in Appendix D. The overall effect on the neutron dose estimate, of the alternative modelling work, is demonstrated to be less than 1 %.

A comparison was also made using the neutron fluence-energy distributions derived from two other ISS shielding models, produced by Sato (Sato 2006) and by Ersmark (Ersmark 2011). As well as utilising different ISS models, they were also for different orbit parameters and heliocentric potentials, and therefore do not constitute a direct comparison to the MTR-2B evaluation using CREME-MCNP, but allow to provide an estimate of the range of variation of results that might be obtained if the model and orbit is not known very accurately. Only the fluence-energy spectra of neutrons were considered for Ersmark's and Sato's data as their proton and helium spectra were not available. Instead, the proton and helium spectra of the CREME + MCNP modelling output were used to enable a full evaluation. The analysis showed differences from the CREME-MCNP neutron dose estimates here, of -1 % and -12 % for Sato and Ersmark respectively (data analysis not shown, but followed the same methodology outlined in Appendix D.

Table 14
Calculated neutron pit rate using DLR GCR + GEANT4 modelling data

Neutron energy distribution	Total neutron fluence rate ($\text{cm}^{-2}\ \text{s}^{-1}$)	Fluence response ($10^{-6}\ \text{cm}^2$)	Pit rate ($10^{-5}\ \text{s}^{-1}$)
DLR GCR + GEANT4[a]	3.538	31.3	11.06 (0.82)

[a] Source: Eakins, 2026

Table 15
Neutron *E*(ISO) response characteristic – based on DLR GCR + GEANT4 modelling data

Neutron energy distribution	*E*(ISO)/Φ[a] (pSv cm^2)	$R_{\Phi\mathrm{Iso}}$[b] (10^{-6} cm^2)	*R*[*E*(ISO)][c] (mSv^{-1})
DLR GCR + GEANT4	263	31.3	119 (9)[d]

a *E*(ISO) fluence to dose conversion coefficient using ICRP 74 data

b isotropic fluence response of the dosemeter

c *E*(ISO) integral dose response characteristic of dosemeter

d half-range using R_Φ envelope of ± 1 standard uncertainty

9 LIMITATIONS TO THE METHOD

When, as here, a dosemeter is used in a radiation field for which it was not originally designed, there will be limitations. Some of these are discussed in this section.

Pits resulting from interactions of charged particles with the nuclei in the detector or holder cannot be subtracted from the neutron-induced signal. This is least problematic for proton interactions with nuclei because recoils from protons and neutrons will behave similarly and hence the established neutron calibration can be used for such proton interactions. Recoils from heavier charged particle interactions with nuclei are more problematic as they won't behave similarly to recoils from neutron interactions. There will hence be double counting of these particles in an overall estimate of dose to an astronaut, if other dosimetry systems used in combination with the UKHSA dosemeter also register this part of the field. Pits due to charged particles interacting via the electronic component of stopping are accounted for, either by the characteristic entry and exit cones ($Z \geq 3$), or by the analytical methods previously described in Section 3 ($Z<3$).

Due to the reduced mass shielding, the charged particle pit accrual rate for outside the ISS will be much higher than for inside; for example, it can be shown (Hager *et al*, 2011) that the calculated proton pit rate outside is an order of magnitude higher. For protons, this can be accounted for, and hence subtracted from the total dosemeter signal with reasonable reliability, using the methods already described in Section 3. For $Z \geq 3$ particles the method for subtracting the signal on dosemeters kept inside the ISS typically uses average daily pit rate data, measured over several short missions. However, the $Z \geq 3$ pit rate for outside the ISS has not been measured and it would be difficult to do so: there have rarely been evaluations where UKHSA dosemeters were exposed purely outside the ISS. The exception to this occurred during MATROSHKA phase 1 (Berger *et al*, 2013), for which the phantom was placed predominantly outside the ISS; however in that case, the overall signal on the dosemeter far exceeded that at which the method to directly measure $Z \geq 3$ particles can be used. As a pragmatic solution, the subtraction method used to correct for the $Z \geq 3$ pit rate outside ISS is hence the same as that used for inside the ISS. For an astronaut EVA dose assessment, the impact of this approximation is generally negligible as the EVA duration is very short compared to the total mission duration. But for the MATROSHKA phase 1 exposure outside of ISS, the impact could be very great, and may even negate the validity of neutron dose assessment in this case.

In addition to the above considerations, the neutron spectrum outside the ISS has not been calculated directly, and it cannot necessarily be assumed that it would be the same as that determined for inside. This is because, although most of the neutrons will still be generated in the ISS hull, their fluence-energy distribution could be different, and their angular distribution would be less isotropic. Nevertheless, the same neutron energy distribution is used to determine the doses for the MATROSHKA phase 1 results and any EVAs that astronauts may perform. The uncertainty resulting from this assumption has not been quantified. The uncertainty on the proton subtraction for EVA is also likely to be high due to large positional variation in mass shielding from the ISS structure.

The above factors unfortunately lead to the conclusion that the neutron assessment for extended exposures outside of the ISS, e.g. during MATROSHKA phase 1, cannot be considered to be as reliable as assessments for inside the ISS. However for astronaut EVAs that are short (typically a half day) whilst overall ISS astronaut mission lengths are long (typically half a year), any added uncertainties from using the dosemeter outside the ISS, where the dosemeter response is less well characterized, are reduced in significance.

10 SUMMARY

The standard-issue UKHSA neutron personal dosemeter has been used in a novel way for assessment of neutron dose on the ISS. Additional procedures have been developed to remove the unwanted signal on the dosemeter from charged particles. Due to the uncertainties associated with doing this, and the use of algorithms for effective dose, the uncertainties on the final neutron dose assessment are large.

The methodology of dosimetry used in this report arose from the simplicity and attractiveness of extending the existing electrochemical etch processing regime already in use at UKHSA to the ISS environment, with subsequent correction factors applied. Other techniques are available (NCRP, 2002), (ICRP, 2013) for estimating doses at LEO conditions, and the method described here is not necessarily considered superior to those other techniques. However, the UKHSA method does have the advantage that it yielded solely a neutron dose estimate, whereas other track etch processing techniques may have difficulty in specifically separating out the neutron dose component.

The nuclear component of stopping of protons produces part of the dosemeter signal, but as this cannot be differentiated from the neutron signal, the results are not purely a neutron dose estimate; rather, it is a ‘neutron and neutron-like interactions of protons’ dose estimate that is given. The contribution from the nuclear component of stopping of protons is expected to be relatively small, but it has not been quantified. Whilst the neutron calibration will be applicable to this type of proton interaction, if other dosimetry systems used alongside the UKHSA dosemeter also see these protons, there will be double counting in the overall assessments of the doses.

Because the UKHSA PADC dosemeter used for the assessments responds to all charged particles above a certain LET threshold, it has been necessary to adjust for the component of the tertiary field (i.e., the particle field within the detector etched volume) that is not due to neutron interactions. This is a significant issue because of the high fluences of protons incident on the ISS, and the high sensitivity of the dosemeter to $Z \geq 3$ particles. Two different methods for the adjustment were used, dependent on the Z of the particle:

- For $Z \geq 3$ particles a fixed number of pits per day has been subtracted from the total pit count, based on the mean of previous directly measured assessments of astronaut doses inside the ISS during short missions. The alternative potential method, i.e. to directly measure this component after application of a secondary chemical etch, was not possible because the signal on the MATROSHKA dosemeters (8000 - 20,000 pits) was significantly above the maximum limit at which that technique can reliably be applied (~1500 pits): at such very high pit densities, it is not practically feasible to identify and align the chemically etched cones from one face of the detector to the other.
- The contribution from $Z<3$ particles had to be calculated via Monte Carlo simulations and analytical methods. The corrections for the $Z=1$ (mainly proton) and $Z=2$ (mainly ^{4}He) contributions to the total number of pits use calculated daily pit rates. Specifically, the subtraction takes into account $Z=1$ ions that were incident on the phantom or the front of the dosemeter, do not then undergo any significant nuclear interactions on their path to the etched volume of the detector, and maintain a minimum $\mathrm{LET}_{\infty,\mathrm{PADC}}$ of 44 keV μm^{-1} for the entirety of their transition through the etched volume. The $Z=2$ contribution has been accounted for similarly, although it is seen to be almost negligible.

Lack of exact knowledge of, for example, parameters such as the LET threshold for the PADC sheet used for a specific measurement, or the exact tissue equivalent shielding from front and rear, will impact on the accuracy of the measurements. However, it has been demonstrated that, within reasonable estimated limits for these parameters, the effect on the neutron dose is acceptable, being within 20 % of the result obtained using the nominal values, and within the other measurement uncertainties.

The effect of using results from more recent modelling (Matthiä *et al*, 2013, Eakins *et al*, 2026) was compared against the results obtained from the original modelling methods that were used during the HAMLET project. It is seen that although the charged particle subtractions, and the absolute calculated neutron fluences, and the dosemeter integral neutron dose response characteristics are different, when all these differences were considered and applied, practically identical neutron dose estimates were produced (Table D.8), irrespective of which modelling method was applied to the data. This gives added confidence in the modelling method used during the original HAMLET project, and in the resultant reported doses (Table 11 and Table 13). In fact, vastly greater variability in dose estimates than this occurred just by varying which dose quantity was used, for which the results can be several tens of percent different.

Following the derivation of the corrections and subtractions, the estimates of the neutron doses made on the ISS using the UKHSA neutron personal dosemeter are improved. Given the magnitude of the total doses received and the significance of the neutron component of the dose, it is clear how this would assist in the overall radiation protection of astronauts. However, the corrections required outside LEO will be different, so if the dosemeter is to be used for more extended missions the corrections will need to be recalculated.

As already noted, the appropriate dose quantity for neutron personal dosemeters in space is something of an open question. ICRP Publication 123 (ICRP, 2013) gives a clear steer towards using a Q(L) based quantity, albeit with two different Q(L) relationships considered; the issues are more connected to the charged particle components of the radiation field, than the neutrons, which do have energy dependent weighting, albeit with w_R. The new operational quantities (ICRU, 2020), ought to escape some of the issues raised in ICRP Publication 123 for neutrons, being effective dose based. But the status of dose quantities might have to wait until the next ICRP Recommendations (Rühm *et al*, 2025), which should reflect the outcomes from Task Group 118, “Relative Biological Effectiveness (RBE), Quality Factor (Q), and Radiation Weighting Factor (w_R)”.

ACKNOWLEDGEMENTS

We thank Guenther Reitz (the PI of the MATROSHKA experiments) for his support and for encouraging us to publish our neutron work. This work was partly funded by the European Commission via the 7th Framework Programme (FP7) under Contract No. 218817 (HAMLET, http://www.fp7-hamlet.eu).

11 REFERENCES

Adams JR, J. (2007) CREME96 update/replacement efforts. Proc. Invited Talk, Single Event Effects Symp.

Bartlett D T, Steele J D, Tanner R J, Gilvin P J, Shaw P V, and Lavelle J (1997). Ten Years On: The NRPB PADC Neutron Personal Monitoring Service. Radiat Prot Dosim, **70** (1–4) 161–163.

Bartlett D T, Hager L G and Tanner R J (2003). Response of a PADC Neutron Personal Dosemeter to HZE: ICCHIBAN-4 Results. 8th Workshop on Radiation Monitoring for the International Space Station, Berkeley, CA, USA. (www.wrmiss.org)

Berger T, Bilski P, Hajek M, Puchalska M, and Reitz G. (2013) The MATROSHKA Experiment: Results and Comparison from Extravehicular Activity (MTR-1) and Intravehicular Activity (MTR-2A/2B) Exposure. Radiation Research, 180(6):622-637 (2013). https://doi.org/10.1667/RR13148.1

Eakins J S, Hager L G, Tanner R J, Berger T, and Matthiä D (2026). Modelling of the neutron and light-ion components of the field inside the International Space Station: support for PADC neutron dose measurements within the HAMLET project. Submitted to Life Sciences in Space Research (*This Issue*).

Ersmark T (2006). Calculated neutron spectrum for the Columbus module. Private communication.

Gilvin P J, Bartlett D T, Shaw P V, Steele J D and Tanner R J (2001). The NRPB PADC neutron personal dosimetry service. Radiat. Prot. Dosim. 96, pp191-5

Hager L G, Tanner R J and Eakins J S (2011). European Commission FP7 contract HAMLET, Work package 1 report, Data Compilation Matroshka 1, 2A, 2B, Neutron Dose Assessment, HPA. European Commission contract report: HAMLET-WP1-REP-003.

Hager L, Tanner, R, Gilvin, P, Eakins, J, Baker, S (2017). The impacts of a new electrochemical etch cycle for the Public Health England neutron personal dosimetry service, *Radiation Measurements* (2017).

ICRU (2020). Operational Quantities for External Radiation Exposure. ICRU Report 95, Vol. 20(1)

ICRP (1977). Recommendations of the ICRP. ICRP Publication 26. Ann. ICRP 1 (3).

ICRP (1996). Conversion Coefficients for use in Radiological Protection against External Radiation. ICRP Publication 74. Ann. ICRP 26 (3-4)

ICRP (2007). The 2007 Recommendations of the International Commission on Radiological Protection. ICRP Publication 103 Ann. ICRP 37 (2-4).

ICRP (2010). Conversion Coefficients for Radiological Protection Quantities for External Radiation Exposures. ICRP Publication 116, Ann. ICRP 40(2-5).

ICRP (2013). Assessment of Radiation Exposure of Astronauts in Space. ICRP Publication 123. Annals of the ICRP **42** (4).

Matthiä D, Berger, T, Mrigakshi, A I, & Reitz, G (2013). A ready-to-use galactic cosmic ray model. Advances in Space Research, 51, 329-338.

NCRP (2002). Operational Radiation Safety Program for Astronauts in Low-Earth-Orbit: A Basic Framework. NCRP Report No 142.

Pelowitz D B (ed.) (2008). MCNPX User's Manual Version 2.6.0. LANL Report: LA-CP-07-1473.

Reitz G and Berger T (2006). *The MATROSHKA Facility—Dose determination during an EVA*. Radiat. Prot. Dosimetry 120, 442–445.

Reitz G *et al* (2009). *Astronaut's Organ Doses Inferred from Measurements in a Human Phantom Outside the International Space Station*. RADIATION RESEARCH 171, 225–235.

Rühm W, Applegate K, Nobuhiko B, Bochud F, Bouffler S, Kun-Woo Cho, Clement C, Gallego E, German O, Hirth G, Makoto Hosono, Michiaki Kai, Laurier D, Senlin Liu, Martinez N, Romanov S, Schneider T, Sutton D and Wojcik A (2025), 'Essentials of the System of Radiological Protection', Journal of Radiological Protection.

Sato T (2011). Calculated neutron spectrum for the ISS. Private communication.

Steele J D, Bhakta J R, Bartlett D T and Tanner R J (1999). Development of a reader for track etch detectors based on a commercially available slide scanner. Radiat Meas, **31**, 179-184.

Straube U, Berger, T, Reitz, G, Facius, R, Fuglesang, C, Reiter, T, Damann, V, Tognini, M. Operational radiation Protection for astronauts and cosmonauts and correlated activities of ESA medical Operations. Acta Astronautica 66 (2010) 963-973.

Tanner R J, Bartlett D T and Hager L G (2001). Recent enhancements to the understanding of the response of the NRPB Neutron Personal Dosemeter. Radiat Meas, **34** (1), 457-461.

Tanner R J (2008). Unpublished data for H_p(10, ISO) up to 20MeV. Private communication.

Tylka A J *et al* (1997). CREME96: A revision of the Cosmic Ray Effects on Micro-Electronics code. IEEE, Trans. Nuc. Sci., 44(6), 2150. Code available from: https://creme.isde.vanderbilt.edu/CREME-MC

Uchihori Y and Benton E R (2007). Results from the ICCHIBAN-3 and ICCHIBAN-4 Experiments to Intercompare the Response of Space Radiation Dosimeters. HIMAC-128. NIRS: Chiba.

Uchihori (2010). Proton irradiations during ICCHIBAN campaign at HIMAC facility, Chiba. Private communication.

Ziegler J F, Ziegler M D and Biersack J P (2008). http://www.srim.org/

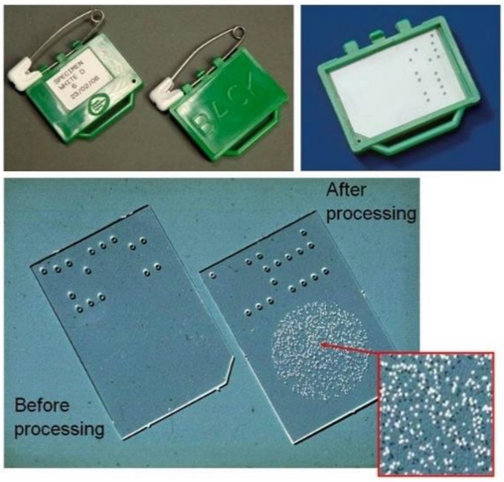

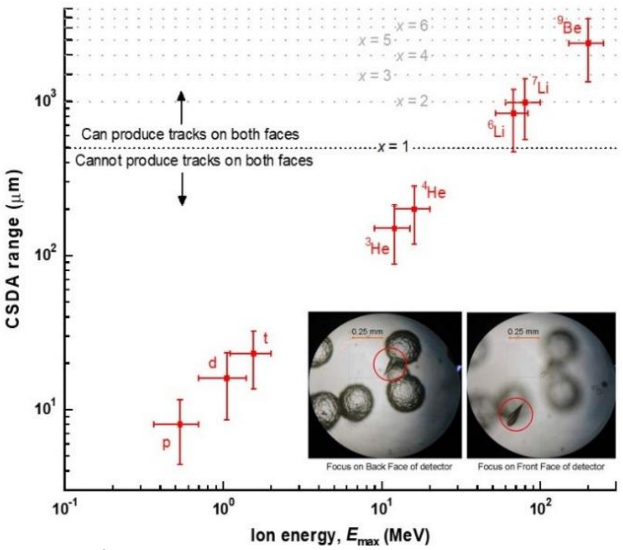

Fig. 1. PADC neutron dosemeter as used in the measurements, before and after electrochemical etch processing. The dosemeter comprises a transparent PADC plastic detector element inserted into a green nylon holder. Once processed the latent tracks produced by the secondaries from neutron interactions are revealed as white spots, also called pits, within the circular processed region. The electrochemical etching is performed on the back face (or 'rear surface') of the detector element. Each dosemeter can be identified by its unique binary dot code number laser engraved onto the detector element

Fig. 2. MCNPX-calculated total n, p, d, t, ^{3}He and α fluence distributions inside the ISS, from exposure to ^{1}H, ^{4}He, ^{12}C and ^{16}O sources (Eakins *et al*, 2026). The data derives from CRÈME generated primary particle source incident on a simplified model of the ISS shielding, using MCNP modelling methods.

Fig. 3. Continuous slowing down approximation (CSDA) range vs E_{max} for different charged particles in PADC. (*Inset*) Chemically etched cones from the passage of a $Z \geq 3$ particle. Data are from SRIM 2008.03, E_{max} is the energy above which the LET is too low for the particle to generate pits (tracks) via direct ionization; the uncertainties show the range for the $LET_{\infty,PADC}$ threshold taking values of 40 and 60 keV μm^{-1}. The thickness of the dosemeter is 500 μm; multiples, *x*, of this thickness are marked as horizontal lines. Note, the y-axis markings are at 500 μm intervals above 1000 μm.

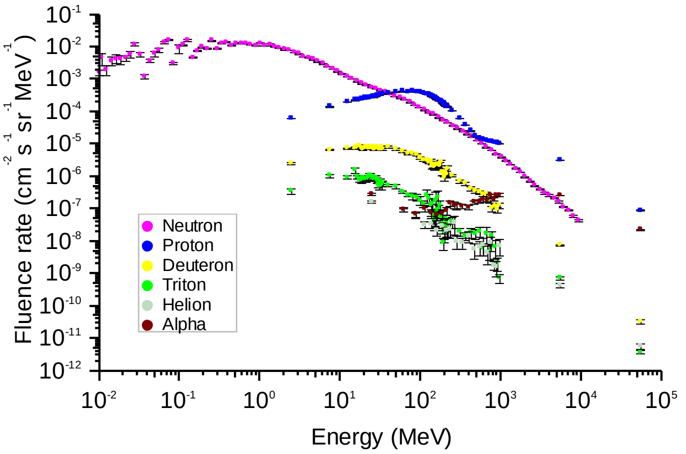

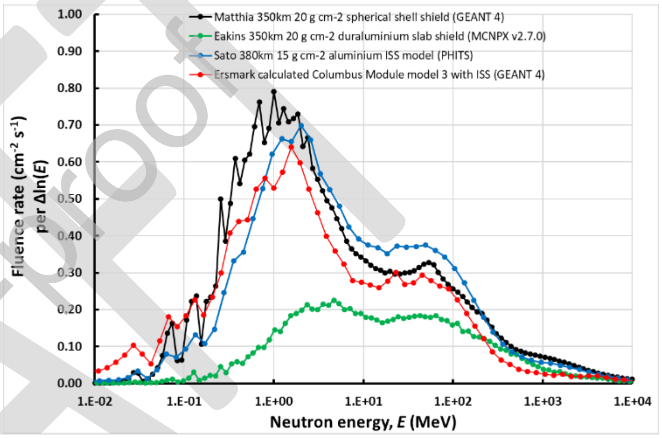

Fig. 4. Monte Carlo calculated neutron energy distributions inside ISS. The Eakins and Matthiä data used the same MTR-2B orbit parameters: their markedly different magnitudes are considered to largely derive from the planar slab shield model used by Eakins which doesn't generate any backscattered neutrons. The Sato and Ersmark data, as well as using different ISS models, are also for different orbit parameters and heliocentric potential

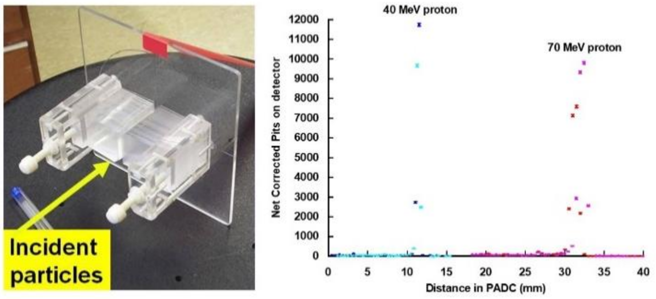

Fig. 5. PADC detector stack arrangement (*left*), and calibration results (*right*) for normally incident protons at HIMAC

Fig. 6. Illustration of the method used to determine the critical range for normally incident protons in PADC (*left*), and assessed proton LET thresholds in PADC for normal incidence irradiations using beams that leave the accelerator with energy E_{ion} (*right*)

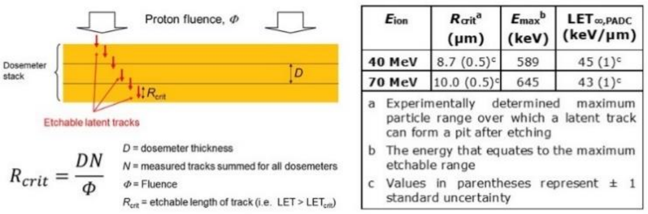

$$R_{crit} = \frac{DN}{\Phi}$$

D = dosemeter thickness
N = measured tracks summed for all dosemeters
Φ = Fluence
R_{crit} = etchable length of track (i.e. LET > LET_{crit})

E_{ion}	R_{crit}[a] (μm)	E_{max}[b] (keV)	$\mathrm{LET}_{\infty,\mathrm{PADC}}$ (keV/μm)
40 MeV	8.7 (0.5)[c]	589	45 (1)[c]
70 MeV	10.0 (0.5)[c]	645	43 (1)[c]

[a] Experimentally determined maximum particle range over which a latent track can form a pit after etching

[b] The energy that equates to the maximum etchable range

[c] Values in parentheses represent ± 1 standard uncertainty

Fig. 7. Fluence response of the dosemeter measured on phantom at NPL at two nominal neutron energies of 70 keV and 100 keV. Individual dosemeters' values distributed across the phantom faces are shown, which indicates that the minimum detectable energy is approximately 50 keV.

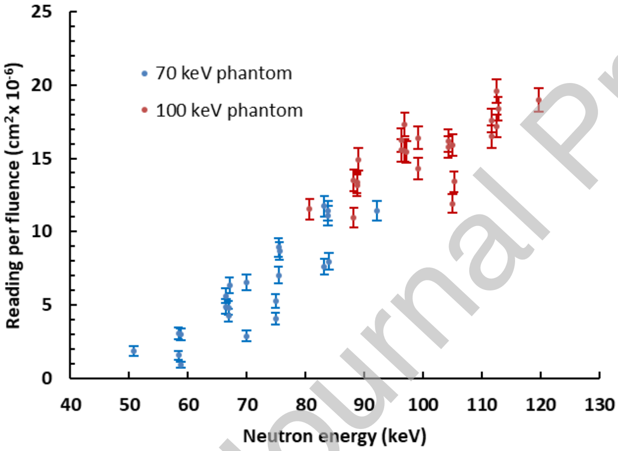

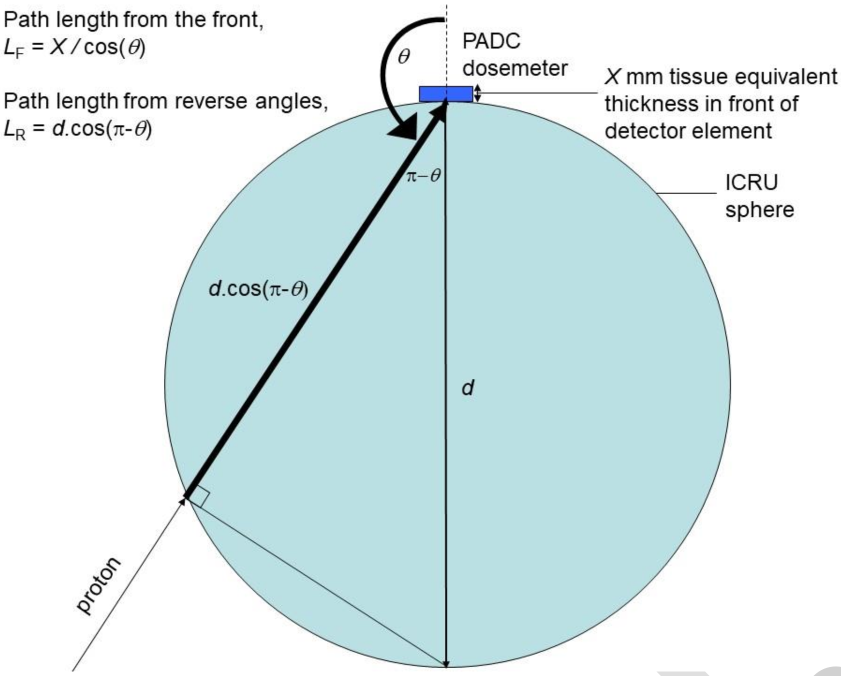

Fig. 8. Path length of a proton through the dosemeter or the ICRU sphere

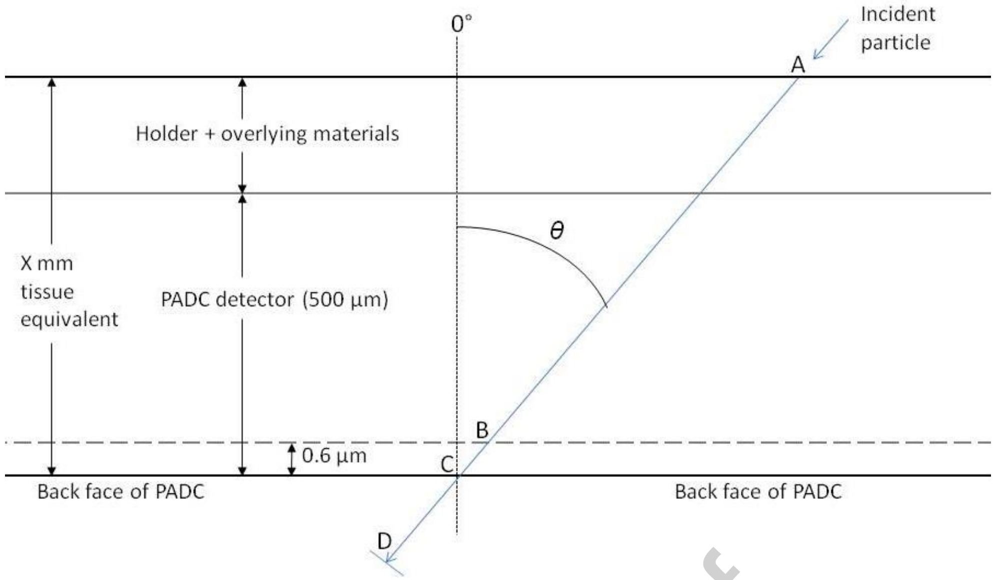

Fig. 9. Geometry for deriving etchable range of particle incident from front through the detector holder

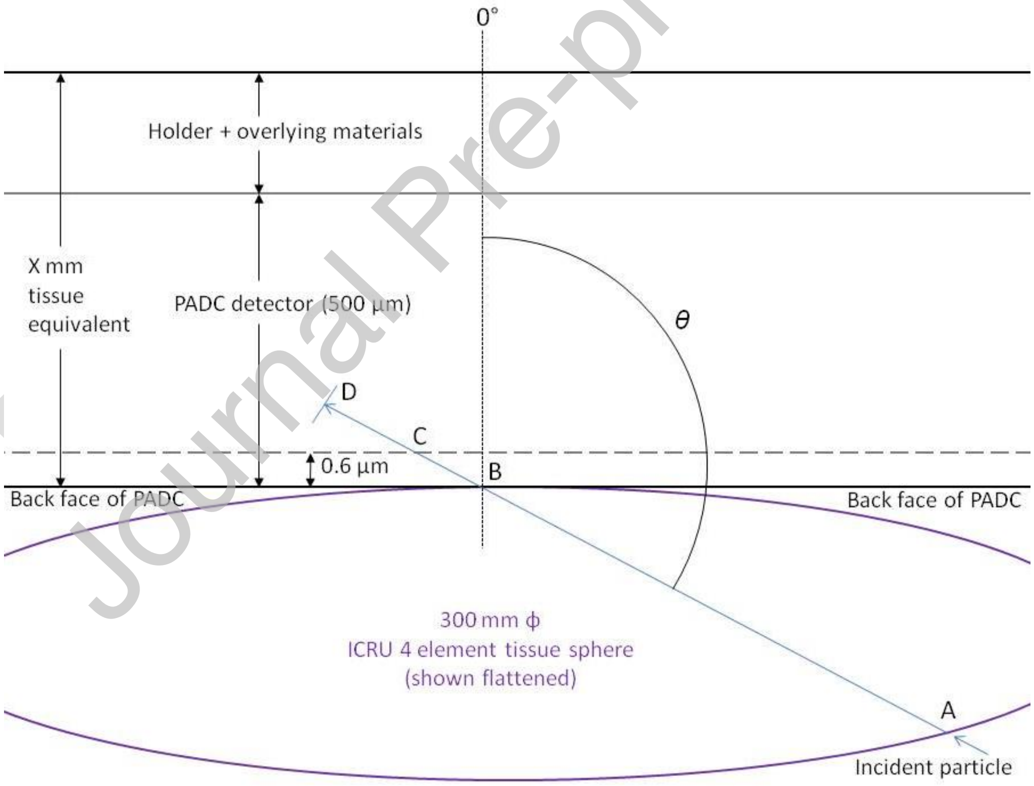

Fig. 10. Geometry for deriving etchable range of particle incident from rear through the ICRU sphere

Appendix A Uncertainties

The uncertainties quoted in Section 6 were derived as below:

- Total pit count, N_{Total}, has an uncertainty of ~15%, arising by adding in quadrature from:
    - random pit counting, equalling twice the square root of the pits counted divided by the pits, giving a value of 3 %
    - variation in sensitivity with detector thickness, giving a value of 13 %
    - linearity correction, giving a value of 6 %.
- $N_{Z\geq3}$ has an uncertainty of approximately 23 %, which is equal to the relative standard deviation on the mean measured value of several assessments.
- $N_{Z<3}$ is simply N_{Total} minus $N_{Z\geq3}$, but the latter two are dependent parameters so its uncertainty cannot be obtained by adding their component uncertainties in quadrature. Instead, a Monte Carlo analysis within Excel was used, assuming N_{Total} and $N_{Z\geq3}$ follow normal distributions, to give an uncertainty in $N_{Z<3}$ of 21 %, as shown in Table 5.
- $C_{Z=0}$ standard uncertainty is 9 %, derived from the half-range of the fluence response envelope for plus and minus 1 standard deviation as shown in Table 1.
- $C_{Z=1}$ uncertainty shown in Table 6 is 29%, and is based on the standard deviation on the calculated pit rates from using a front thickness covering range of 6.5 – 10.0 mm, a sphere diameter range of 200 – 300 mm and an LET threshold range of 40 – 48 keV µm^{-1}. Whilst the above ranges provided an uncertainty that was considered appropriate during the HAMLET project for a best estimate, the front covering and LET threshold ranges have since been broadened to quantify the possible impact of these parameters at their minimum and maximum expected limits (as discussed under 'tissue shielding thickness' and 'LET threshold' below).
- $C_{Z=2}$ uncertainty shown in Table 6 is obtained in the same way as for for $C_{Z=1}$, except the LET threshold range used is that appropriate for helium ions.
- $N_{Z=0}$ uncertainty is obtained from considering the uncertainties on the components in Equation 2. $C_{Z=0}$ and $C_{Z<3}$ are dependent parameters, and so the uncertainty in their ratio $C_{Z=0}$ /$C_{Z<3}$ cannot be obtained by adding them in quadrature. Instead a Monte Carlo analysis within Excel was used, assuming $C_{Z=0}$, $C_{Z=1}$ and $C_{Z=2}$ follow normal distributions. This uncertainty is then added in quadrature to the uncertainty on $N_{Z<3}$. Because $C_{Z=0}$ is a very dominant component of $C_{Z<3}$, the uncertainty on the ratio $C_{Z=0}$ /$C_{Z<3}$ is relatively low, being ~9 %, and when combined with the 21 % uncertainty on $N_{Z<3}$, the uncertainty on $N_{Z=0}$ becomes 23 %.
- $N_{Z=1}$ and $N_{Z=2}$ uncertainties are obtained in the same way as for $N_{Z=0}$. Their relative uncertainties are much larger than those for $N_{Z=0}$ because the $C_{Z=1}$ and $C_{Z=2}$ contributions to $C_{Z<3}$ are much lower.
- The uncertainty on the dose response characteristic of the dosemeter, $R_{E(\mathrm{ISO}),\ \mathrm{ISS}}$, defined in Equation 5, is 8 %. It is the half-range from using a fluence response envelope of plus and minus one standard uncertainty, as shown in Table 8.
- The uncertainty on E(ISO), the final neutron dose estimate, is 24 %, and is derived by combining the uncertainties on the component s shown in Equation 6 in quadrature.

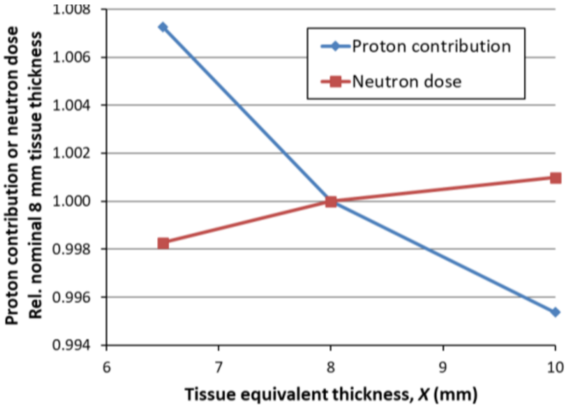

Appendix B Sensitivity analysis

In this section, potential variations in certain parameters are evaluated in terms of their effect on the neutron dose determination.

Monte Carlo and CREME outputs

The method to characterize the dosemeter relies on energy distributions generated by Monte Carlo modelling, which in turn depend on the primary field ion energy distributions generated by the CREME96 package. CREME has its own set of input parameters that can be varied, e.g., ISS altitude, geomagnetic transmission function etc. These latter parameters have been kept at fixed values for the assessment of the doses during all MATROSHKA phases. The impact of varying some of the CREME input parameters has been discussed elsewhere (Eakins *et al*, 2026), however, it is difficult to fully quantify the effect of this on the final neutron dose. The input parameters were optimised to generally match those pertaining during the MATROSHKA phases.

Tissue shielding thickness

The nominal arrangement modelled, as shown in Fig. 8, is a PADC dosemeter located on the ICRU 4 element tissue phantom of diameter 300 mm. The etched face of the PADC detector has *X* mm of tissue equivalent material in front of it. Based on information provided during the ESA-MATROSHKA project, the thickness *X* is estimated nominally as 8 mm for MATROSHKA 2A and 2B and 11.7 mm for MATROSHKA 1. Varying the thickness range used with the methods described in Section 3 makes only moderate change to the proton contribution and much less effect on the neutron dose, Fig. B.1. Variation in the front thickness covering hence cannot impact the neutron dose significantly.

The impact of choosing the ICRU sphere as a replacement for a human torso, in terms of its attenuating effect, can be assessed by changing its diameter, which also indicates the impact of the different builds of astronaut who might wear the dosemeter. Applying the methods described in Section 3, a reduction of the diameter to only 200 mm increases the total proton contribution by around 8% but the neutron dose only reduces by 1.3%. Given that typical astronaut build may not vary significantly outside the presumed 200-300 mm range, it is unlikely that the neutron dose will be impacted by more than a few per cent by varying this parameter.

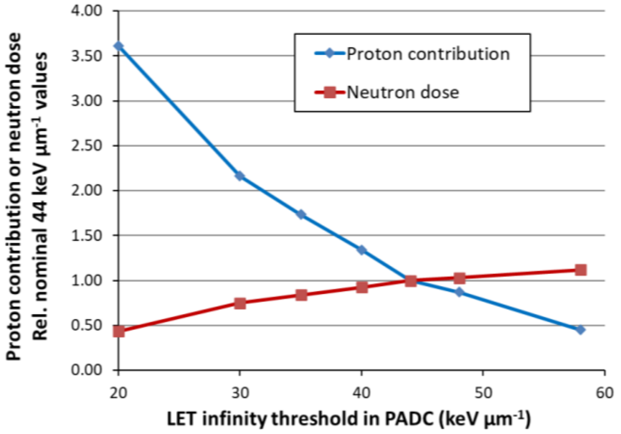

Fig. B.1: Effect of variation in thickness of front covering material on proton contribution and neutron dose

LET threshold

The LET threshold is not measured for each assessment. In fact, it has only rarely been assessed, but a modest change in LET threshold can be shown to have large effects on the proton contribution. A change in LET threshold will change the width of the detectable proton energy window, and consequently the calculated number of protons detected. Because of the normalizing methods used (Equation 2), the neutron component is inversely proportional to the sum of the calculated pits from all $Z<3$ particles, so changes in the calculated proton pits will directly affect the final neutron contribution and hence neutron dose. Fig. B.2 shows how changes to the LET threshold affect the proton and neutron contributions. The measured proton LET threshold is 44 keV μm^{-1}, but it is recognised that this was established using a limited number of PADC sheets from specific batches of PADC, and it is conceivable that for PADC manufactured at much later dates this value could show variation. The degree to which changes, such as to detector materials and processing regimes, could affect the LET threshold remains unknown: the current LET threshold was obtained using an older detector material and processing regime.

Fig. B.2: Effect of variation in proton LET threshold on proton contribution and neutron dose

Given the above unknowns, it is difficult to be certain if the full range of LET values shown in Fig. B.2 are likely. As well as the LET thresholds of 44 keV μm^{-1} for protons and 58 keV μm^{-1} for ^{4}He ions, it has also previously been measured for ^{20}Ne ions to be less than 56 keV μm^{-1} and for ^{12}C ions at ~80 keV μm^{-1} (Hager *et al*, 2011). It is clear from Fig. B.2 that increasing the proton LET threshold above the nominal 44 keV μm^{-1} value only increases the neutron dose slightly, but a more significant effect is seen if the threshold is reduced below the nominal value. If it is reduced to around 20 keV μm^{-1}, the neutron dose would be approximately halved relative to use of the nominal threshold value of 44 keV μm^{-1}. But an LET threshold of 20 keV μm^{-1} would be considered very low for an electrochemical etch processing regime, so it is unlikely that quite this degree of difference would be seen. Nevertheless, it could potentially be used as an outside limit to state that the neutron dose may overestimate by up to a factor of two. Conversely, from Fig. B.2, any underestimate is likely to be no more than 20 %.

For helium ions a reduction of the LET threshold from 58 keV μm^{-1} to 20 keV μm^{-1} increases their contribution by a factor of eighteen, but only reduces the neutron dose by 5 %. As Table 7 shows, this is because their contribution to the signal at an LET threshold of 58 keV μm^{-1} is very low to start with. It can hence be concluded that uncertainties in the LET threshold for helium ions will not impact the neutron dose significantly.

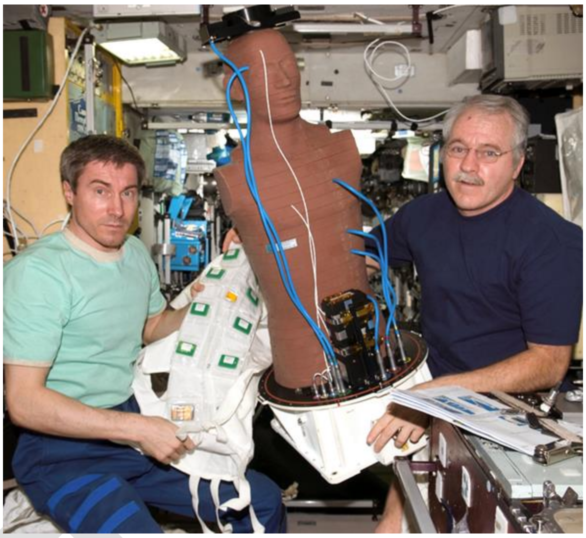

Appendix C MATROSHKA poncho jacket: individual dosemeter pit counts

The positions of dosemeters in the poncho waistcoat are shown for the three MATROSHKA (MTR) phases in Figs C.1 to C.3, and next to the MTR phantom in Fig C.4. The individual dosemeter net corrected pit counts for the poncho and reference dosemeters are given in Tables C.1 to C.3.

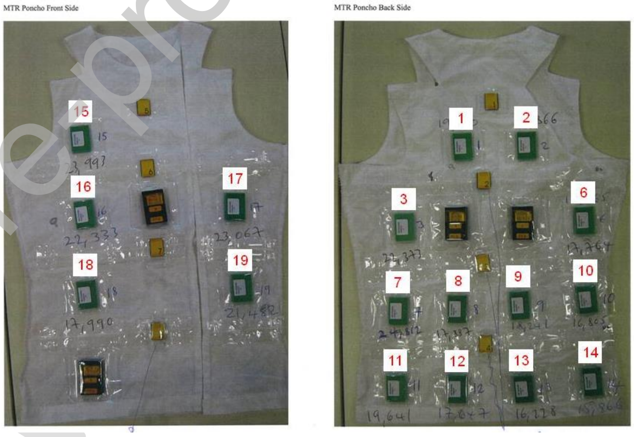

Fig. C.1 MTR-1 poncho waistcoat, front (left) and back (right)

Fig. C.2 MTR-2A Poncho waistcoat, front (left) and back (right)

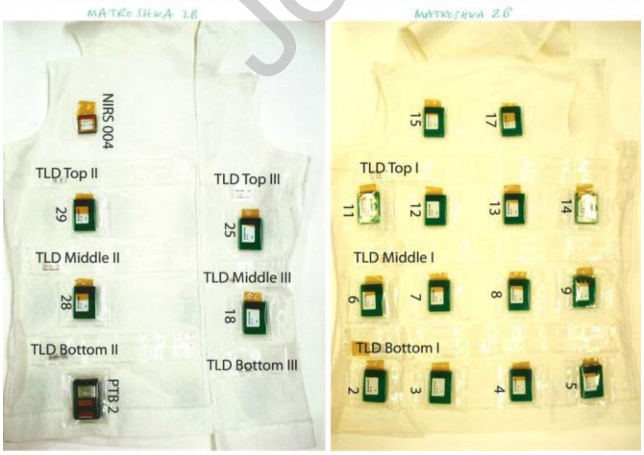

Fig. C.3 MTR-2B poncho waistcoat, front (left) and back (right)

Fig. C.4 UKHSA Neutron dosemeters (green) attached to poncho waistcoat, and the Matroshka phantom, inside ISS

Table C.1 Assessed pits on dosemeters for MTR-1

Location	ID	Dtr No	N_{Total}[a]
	15	D112903	23993
	16	D112990	22332
	17	D112948	23067
	18	D112955	17990
	19	D112943	21481
	1	D112974	19929
	2	D112960	17866
	3	D112971	22373
	6	D112968	17764
	7	D112938	24810
	8	D112959	17887
	9	D112973	18240
	10	D112902	16805
	11	D112988	19641
	12	D112972	17645
	13	D112987	16228
	14	D112965	15864
Mean for poncho			19642 (2946)[b]
	20 (sewed in)	D112979	8644 (1297)[b]
	25 (MTR Ref 2)	D112964	10046 (1507)[b]
Mean for reference box			9345 (1402)[b]

[a] measured total pit count corrected for linearity and background subtracted

[b] estimated random uncertainty from pit counting, variation in sensitivity with detector thickness, and linearity correction

Table C.2 Assessed pits on dosemeters for MTR-2A

Location	ID	Dtr No	N_{Total}[a]

Poncho Front	5	D119178	8189
	4	D119168	8900
	7	D119154	9121
	21	D119138	9313
	10	D119134	10621
	14	D119116	Processing error
	19	D119163	Processing error
	20	D119112	8201
	17	D119166	9491
	18	D119142	9652
	16	D119164	9737
	15	D119182	9904
	23	D119101	8817
	22	D119130	8861
	28	D119151	9209
	29	D119103	9451
	25	D119175	9737
	26	D119167	9851
	24	D119158	9959
	27	D119170	Processing error
Mean for poncho			9354 (1403)[b]
Reference Box	3	D119172	9257 (1389)[b]
a	measured total pit count corrected for linearity and background subtracted		
b	estimated random uncertainty from pit counting, variation in sensitivity with detector thickness, and linearity correction		

Table C.3 Assessed pits on dosemeters for MTR-2B

Location	ID	Dtr No	N_{Total}[a]
	29	A401569	8315
	25	A401549	8295
	28	A401580	8167
	18	A401537	7886
	12	A401573	7034
	13	A401568	7396
	11	A401501	7641
	15	A401585	8285
	17	A401588	8423
	14	A401518	8803
	6	A401564	7721
	2	A401546	8009
	7	A401576	8170
	3	A401579	8175
	8	A401571	8375
	4	A401578	8707
	9	A401540	8842
	5	A401554	9205
Mean for poncho			8192 (1229)[b]
Reference Box	16(ntdp7,ref 2)	A401582	7030 (1055)[b]

[a] measured total pit count corrected for linearity and background subtracted

[b] estimated random uncertainty from pit counting, variation in sensitivity with detector thickness, and linearity correction

Appendix D Comparison of Matroshka-2B neutron doses obtained using CRÈME + MCNP modelling results and DLR GCR + GEANT4 modelling results

A re-evaluation of the MATROSHKA 2B neutron dose determination has been performed using alternative particle spectra data supplied by DLR (Matthiä *et al*, 2013) obtained from using DLR GCR + GEANT4 modelling. The re-evaluation is compared here against the results obtained using the CREME + MCNP modelling performed during the HAMLET project. As in Section 6, the following comparison tables use the MATROSHKA 2B mean pit density as their basis, and are ordered in the same way to aid identifying where the data originated from and what they relate to. For more detailed table descriptions see Section 6.

Table D.1
Calculated neutron pit rate

Neutron energy distribution	Pit rate (10^{-5} s^{-1})
CREME + MCNP[a]	4.68 (0.41)[c]
DLR GCR + Geant 4[b]	11.06 (0.82)[c]

a From CRÈME + MCNP modelling: Source: Eakins, 2026

b From DLR GCR + GEANT4 modelling: Source: Eakins, 2026; Matthiä, 2013

c half-range using R_{Φ} envelope of ± 1 standard uncertainty

Table D.2
Calculated neutron pits on detector, $C_{Z=0}$

Neutron energy distribution	Calculated neutron pit rate (d^{-1})	Exposure duration (d)	Calculated neutron pits on detector $C_{Z=0}$
CREME + MCNP[a]	4.04 (0.36)[c]	404	1634 (144)
DLR GCR + Geant 4[b]	9.56 (0.71)[c]	404	3861 (286)

a From CRÈME + MCNP modelling: Source: Eakins, 2026

b From DLR GCR + GEANT4 modelling: Source: Eakins, 2026; Matthiä, 2013

c half-range using R_{Φ} envelope of ± 1 standard uncertainty

The greater than factor of two difference between the MCNP and GEANT calculated neutron pits, $C_{Z=0}$, is mostly a reflection of the higher total neutron fluence rate found in the GEANT modelling compared with the fluence rate from the MCNP modelling. (Eakins *et al*, 2026), as demonstrated in Fig.4.

Table D.3
Charged particle pits on detector (MCNP)

Particle type	Pit rate (d^{-1})	Exposure duration (d)	Pits on detector
$Z \geq 3$	4.3 (1.0)	404	1737 (404)
$Z = 1$	1.58 (0.46)	404	638 (186)
$Z = 2$	0.027 (0.024)	404	11 (10)

When comparing the values obtained using MCNP modelling data generated during the HAMLET project (Table D.3), against the GEANT modelling data (Table D.4), some observations can be made. Firstly, the $Z \geq 3$ value used with the GEANT4 data is larger because more independent measurements of this component were available when the GEANT data were supplied. As can be seen from Table D.5, the effect of this difference on $N_{Z<3}$ is small because the total net pits, N_{Total}, is much larger than the $Z \geq 3$ pits. Secondly, the calculated $Z=1$ values differ by only 2.5 %, and are certainly well within statistical uncertainty. Finally, the $Z=2$ values show a factor of two difference, but the magnitude of the pits is very low, so the overall impact of this difference on the neutron dose assessment is negligible.

Table D.4
Charged particle pits on detector (GEANT4)

Particle type	Pit rate (d^{-1})	Exposure duration (d)	Pits on detector
$Z \geq 3$	4.72 (1.03)	404	1907 (416)
$Z = 1$	1.62 (0.47)	404	654 (190)
$Z = 2$	0.054 (0.048)	404	22 (19)

Table D.5
Measured pits on the detector

Data source	N_{Total}[a]	$N_{Z\geq3}$[b]	$N_{Z<3}$[c]
CREME + MCNPHAMLET	8047 (1229)	1737 (404)	6309 (1306)
DLR GCR + Geant 4	8047 (1229)	1907 (416)	6140 (1302)

a total net pits after linearity and background correction

b measured pits from $Z \geq 3$ particles

c estimated pits left from $Z<3$ particles

Table D.6
Measured vs. calculated pits for $Z<3$ particles

Data source	Measured pits	Calculated pits			Sum
	$N_{Z<3}$[a]	$C_{Z=0}$[b]	$C_{Z=1}$[c]	$C_{Z=2}$[d]	$C_{Z<3}$[a]
CRÈME	6309	1634	638	11	2283
+ MCNP	(1306)	(144)	(186)	(10)	(235)
DLR GCR	6140	3861	654	22	4538
+ Geant 4	(1302)	(286)	(190)	(19)	(344)

a measured or calculated pits from $Z<3$ particles

b calculated pits from $Z=0$ (neutrons)

c calculated pits from $Z=1$ (protons, deuterons, tritons), obtained by method in Section 3

d calculated pits from $Z=2$ (alphas and helions), obtained by method in Section 3

Table D.7
Measured pits for all particles

Data source	N_{Total}[a]	$N_{Z\geq3}$[b]	$N_{Z=0}$[c]	$N_{Z=1}$[d]	$N_{Z=2}$[e]
CREME+ MCNP	8047	1737	4515	1764	30
	(1229)	(404)	(1016)	(546)	(24)
DLR GCR	8047	1907	5225	886	30
+ Geant 4	(1229)	(416)	(1131)	(297)	(23)

a measured total pits after linearity and background correction

b measured pits from $Z\geq3$ particles

c corrected pits from $Z=0$ (neutrons)

d corrected pits from $Z=1$ (protons, deuterons, tritons)

e corrected pits from $Z=2$ (alphas, helions)

It will be observed in Table D.6 that $C_{Z=0}$ is a factor of 2.36 higher using Matthiä's data (3861 pits vs 1634 pits). But because for both data sources the calculated neutron pits dominate the summation of all $Z<3$ pits, and the ratio $C_{Z=0}$ / $C_{Z<3}$ is similar for both data sources, then when Equation 2 is applied it results in a 16% difference, i.e., not very dissimilar values, for $N_{Z=0}$ (Table D.7).

Table D.8
Measured E(ISO)

Neutron energy distribution	**$N_{Z=0}$**[a]	**$R[E(\mathrm{ISO})]$**[b] **(mSv^{-1})**	**$E(\mathrm{ISO})$**[c] **(mSv)**
CRÈME + MCNP[d]	4515 (1016)	102 (8)	44.3 (10.6)[f]
DLR GCR + Geant 4[e]	5225 (1131)	119 (9)	43.9 (10.0)[f]

a corrected pits from $Z=0$ (neutrons)

b *E*(ISO) integral dose response characteristic of dosemeter

c Assessed *E*(ISO)

d From CRÈME + MCNP modelling: Source: Eakins, 2026

e From DLR GCR + GEANT4 modelling: Source: Eakins, 2026; Matthiä, 2013

f combined standard uncertainty: on integral dose response characteristic; $Z\geq3$, $Z=1$, $Z=2$ particle subtractions; and random uncertainty on pit counting, half-range using R_{Φ} envelope of ± 1 standard uncertainty

The overall effect of applying the GEANT4 datasets to re-evaluate the MATROSHKA 2B neutron dose is assessed to be less than 1 %, and due to the large uncertainties, statistically, the two determinations are not separable (Table D.8). The large, approximately 25% standard uncertainties, mean that there can't be a high level of confidence in the accuracy of the assessed neutron doses. it can potentially range over quite a wide spread of values.

Declaration of Interest Statement

☒ The authors declare that they have no known competing financial interests or personal relationships that could have appeared to influence the work reported in this paper.